Supporting Information for:

Integration of Chiral Phosphine Ligand and Ionic Liquids: Sustainable and Functionally Enhanced BINAP-Based Chiral Ru(II) Catalysts for Enantioselective Hydrogenation of *β*-Keto Esters

Fan Wang,[a,b] Shuai Zhang,[b] Sen Huang,[b] Lin Zhu,[b] Hongbing Song,[b] Congxia Xie[a] and Xin Jin*[,b]

[a] College of Chemistry and Molecular Engineering, Qingdao University of Science and Technology, 53 Zhengzhou Road, Qingdao 266042, China

[b] College of Chemical Engineering, Qingdao University of Science and Technology, 53 Zhengzhou Road, Qingdao 266042, China

Corresponding Author:

* *E*-mail: Xin Jin, jinx1971@163.com

List of the contents

1 Experimental Procedures

1.1 Synthesis and characterization of **2a**

Under an argon atmosphere, $Me(EO)_{16}OMs$ (10.0 g, 12.3 mmol) and N-methyl imidazole (1.35 g, 16.4 mmol) were mixed in toluene (30 mL), and then the mixture was heated to 95 °C and stirred for 30 h. After removing the solvent under reduced pressure, the excess N-methyl imidazole was extracted with methyl tert-butyl ether (5 × 10 mL). The residual solvent was removed to obtained $[Me(EO)_{16}MIM][OMs]$ (**2a**) as an orange-yellow viscous liquid. Yield: 9.7 g, 88%. Characterization: ^{1}H NMR (500.0 MHz, $CDCl_3$)：δ (ppm) = 9.780 (s, 1H, CH_{im}), 7.666 (s, 1H, CH_{im}), 7.396 (s, 1H, CH_{im}), 4.519 (t, 2H, J = 5 Hz, N-CH_2CH$_2$), 4.010 (s, 3H, N-CH_3), 3.874 (t, 2H, J = 5 Hz, N-CH$_2$CH_2), 3.658-3.540 (m, 68H, OCH_2CH_2O), 3.379 (s, 3H, OCH_3), 2.784 (s, 3H, $CH_3SO_3^-$); ^{13}C NMR (150.9 MHz, $CDCl_3$)：δ (ppm) = 138.232, 123.663, 122.871, 71.944, 70.614-70.496, 70.391, 70.216, 59.046, 49.565, 39.624, 36.288; MS (ESI positive): m/z = 801.51, calcd for $C_{37}H_{73}O_{18}N_2$ ($[Me(EO)_{16}MIM]^+$): 801.98; MS (ESI negative): m/z = 94.98, calcd for CH_3O_3S ($[CH_3SO_3]^-$): 94.98.

1.2 Synthesis and characterization of $Ph(CH_2)_2OMs$

A solution of methanesulfonyl chloride (6.7 ml, 86.1 mmol) in toluene (30 mL) was added dropwise to a vigorously stirred solution of $Ph(CH_2)_2OH$ (10.5 g, 86.1 mmol), Et_3N (12.0 ml, 86.1 mmol) and toluene (40 mL) at 0 °C. After adding MsCl, the mixture was stirred at 30°C for 24, followed by a filtration. The filtrate was evaporated under vacuum to afford $Ph(CH_2)_2OMs$ as a light yellow liquid. Yield: 16.2 g, 99%. Characterization: ^{1}H NMR (500.0 MHz, $CDCl_3$): δ (ppm) = 7.314 (t, 2H, J = 7.5 Hz, Ph-H), 7.262-7.218 (m, 3H, Ph-H), 4.398 (t, 2H, J = 7.0 Hz, PhCH$_2$CH_2OMs), 3.033 (t, 2H, J = 7.0 Hz, PhCH_2CH$_2$OMs), 2.806 (s, 3H, OSO$_2$CH_3).

1.3 Synthesis and characterization of **6**

Under an argon atmosphere, $Ph(CH_2)_2OMs$ (2.88 g, 14.4 mmol) and N-methyl imidazole (1.54 g, 18.8 mmol) were mixed in toluene (30 mL), and then the mixture was heated to 95 °C and stirred for 48 h. After removing the solvent under reduced pressure, the excess N-methyl imidazole was extracted with methyl tert-butyl ether (5 × 10 mL). The residual solvent was removed to obtained $[Ph(CH_2)_2MIM][OMs]$ (**6**) as an orange-red viscous liquid. Yield: 4.0 g, 98%. Characterization: ^{1}H NMR (500.0 MHz, DMSO-d_6): δ (ppm) = 9.060 (s, 1H, CH_{im}), 7.730 (s, 1H, CH_{im}), 7.674 (s, 1H, CH_{im}), 7.312 (t, 2H, J = 7.5 Hz, Ph-H), 7.258-7.210 (m, 3H, Ph-H), 4.431 (t, 2H, J = 7.5 Hz, PhCH$_2$CH_2N), 3.816 (s, 3H, N-CH_3), 3.127 (t, 2H, J = 7.5 Hz, PhCH_2CH$_2$N), 2.306 (s, 3H, C$H_3SO_3^-$); ^{13}C NMR (125.7 MHz, $CDCl_3$): δ (ppm) = 137.599, 136.169, 128.902, 128.807, 127.277, 123.297, 122.320, 50.790, 39.711, 36.358, 36.247; HRMS (ESI positive): m/z = 187.1232, calcd for $C_{12}H_{15}N_2$ ($[Ph(CH_2)_2MIM]^+$): 187.1230; HRMS (ESI negative): m/z = 94.9811, calcd for CH_3O_3S ($[CH_3SO_3]^-$): 94.9808.

1.4 Synthesis and characterization of **3a**

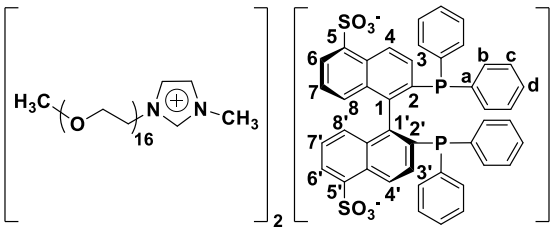

3a

Under an argon atmosphere, $[Me(EO)_{16}MIM][OMs]$ (1.0 g, 1.1 mmol) and (*S*)-BINAP-$(SO_3Na)_2 \cdot 5H_2O$ (0.6 g, 0.65 mmol) were

mixed in acetonitrile (15 mL) with vigorous stirring at ambient temperature for 144 h, followed by a filtration. The filtrate was evaporated to obtained [$Me(EO)_{16}MIM]_2$[(*S*)-BINAP-($SO_3)_2$] (**3a**) as a yellow viscous liquid. Yield: 1.3 g, 97%. The ^{1}H NMR spectrum analysis revealed that the mass fractions of residual CH_3SO_3Na in **3a** was 1.1%. Characterization: $[\alpha]_D^{14}$= -20.08 (*c* 0.05, CH_3OH); ^{1}H NMR (500.0 MHz, $CDCl_3$): *δ* (ppm) = 9.776 (s, 2H, CH_{im}), 9.054 (d, 2H, *J* = 9.0 Hz, 4,4'-H), 8.087 (t, 2H, *J* = 4.0 Hz, 7,7'-H), 7.574 (s, 2H, CH_{im}), 7.476 (d, 2H, *J* = 9.0 Hz, 3,3'-H), 7.226 (s, 2H, CH_{im}), 7.158-7.032 (m, 20H, Ph-H), 6.834 (d, 4H, *J* = 4.0 Hz, 6,6'-H and 8,8'-H), 4.450 (t, 4H, *J* = 4.5 Hz, N-CH_2CH_2O), 3.899 (s, 6H, N-CH_3), 3.811 (t, 4H, *J* = 4.5 Hz, N-CH_2CH_2O), 3.657-3.539 (m, 141H, OCH_2CH_2O), 3.378 (s, 6H, OCH_3); ^{13}C NMR (150.9 MHz, $CDCl_3$): *δ* (ppm) = 145.568 (m, 1,1'-C), 141.851 (s, 5,5'-C), 137.952, 137.902 (s, 2,2'-C), 137.360 (m, a-C), 135.148 (d, 9,9'-C), 134.112 (m, d-C), 133.014 (m, c-C), 131.641 (s, 3,3'-H), 130.276 (s, 8,8'-C), 129.566 (s, 10,10'-C), 128.383 (s, b-C), 128.177-128.080 (m, c-C), 127.644 (s, b-C), 127.101 (s, 4,4'-C), 126.205 (s, 6,6'-C), 124.213 (s, 7,7'-C), 123.580, 122.840, 71.953, 70.607-70.480, 70.364, 70.197, 69.056, 49.632, 39.601, 36.347; ^{31}P NMR (202.4 MHz, D_2O): *δ* (ppm) = -16.127; HRMS (ESI positive): *m*/*z* = 801.4952, calcd for $C_{37}H_{73}O_{16}N_2$ ([$Me(EO)_{16}MIM]^+$): 801.4955; HRMS (ESI negative): *m*/*z* = 781.1022, calcd for $C_{44}H_{31}O_6P_2S_2$ ([(*S*)-BINAP-($SO_3)_2$ + H]$^-$): 781.1043.

1.5 Synthesis and characterization of **7**

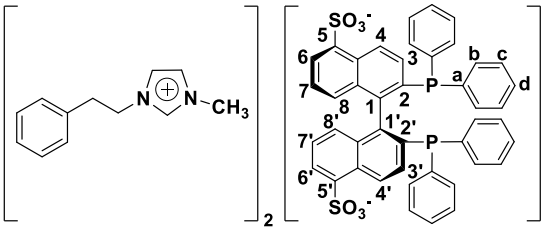

7

Under an argon atmosphere, [$Ph(CH_2)_2MIM$][OMs] (0.81 g, 2.9 mmol) and (*S*)-BINAP-($SO_3Na)_2\cdot5H_2O$ (1.7 g, 1.8 mmol) were mixed in acetonitrile (15 mL) with vigorous stirring at ambient temperature for 72 h, followed by a filtration. After the filtrate was evaporated, chloroform (10 ml) was added and the mixture was stirred at ambient temperature for 0.5 h until a white precipitate was formed. The precipitate was filtered and washed with chloroform (1 mL×2) to obtained [$Ph(CH_2)_2MIM]_2$[(*S*)-BINAP-($SO_3)_2$] (**7**) as a white solid powder. Yield: 0.2 g, 12%. The ^{1}H NMR spectrum analysis revealed that the mass fractions of residual CH_3SO_3Na in **7** was 1.0%. Characterization: $[\alpha]_D^{20}$= -65.92 (*c* 0.05, CH_3OH); ^{1}H NMR (500.0 MHz, CD_3OD): *δ* (ppm) = 8.928 (d, 2H, *J* = 9.0 Hz, 4,4'-H), 8.702 (s, 1H, N=CH-N, active hydrogen), 7.984 (d, 2H, *J* = 6.5 Hz, 6,6'-H), 7.503-7.469 (m, 6H, CH_{im} and 3,3'-H), 7.276 (t, 4H, *J* = 7.5 Hz, $(CH_2)_2$Ph-H), 7.243-7.192 (m, 10H, $(CH_2)_2$Ph-H and P-Ph-H), 7.147-7.090 (m, 12H, $(CH_2)_2$Ph-H and P-Ph-H), 7.010 (t, 4H, *J* = 7.0 Hz, P-Ph-H), 6.801 (t, 2H, *J* = 8.5 Hz, 7,7'-H), 6.744 (d, 2H, *J* = 8.5 Hz, 8,8'-H), 4.434 (*t*, 4H, *J* = 7.0 Hz, $PhCH_2CH_2N$), 3.818 (s, 6H, N-CH_3), 3.137 (t, 4H, *J* = 7.0 Hz, $PhCH_2CH_2N$); ^{13}C NMR (150.9 MHz, CD_3OD): *δ* (ppm) = 146.248 (m, 1,1′-C), 142.088 (s, 5,5′-C), 139.069-138.985 (m, a-C), 137.867, 137.796-137.713 (m, a-C), 137.777, 137.550 (d, 2,2′-C), 135.465 (m, d-C), 135.252 (m, 9,9′-C), 133.973 (m, c-C), 132.206 (s, 3,3′-C), 131.391 (s, 8,8′-C), 130.492 (s, 10,10′-C), 129.952, 129.880 (s, b-C), 129.795, 129.435-129.385 (m, c-C), 129.327-129.291 (m, c-C), 129.072 (s, b-C), 128.328, 127.936 (s, 4,4′-C), 127.269, 125.352, 124.812 (s, 6,6′-C), 123.705 (s, 7,7′-C), 51.967, 37.156, 36.332; ^{31}P NMR (202.4 MHz, CD_3OD): *δ* (ppm) = -15.293; HRMS (ESI positive): *m*/*z* = 187.1235, calcd for $C_{12}H_{15}N_2$ ([$Ph(CH_2)_2MIM]^+$): 187.1230; HRMS (ESI negative): *m*/*z* = 390.0486 (z=2), calcd for $C_{44}H_{30}O_6P_2S_2$ ([(*S*)-BINAP-($SO_3)_2]^{2-}$): 390.0485.

1.6 Typical procedure for recycling CRTP-PolyIMILsRuBr$_2$ catalysts under the HCBS system

Typically, **3b** (7.9 mg, 0.00313 mmol) and [Ru(COD)(2-methylallyl)$_2$] (1.0 mg, 0.00313 mmol) were dissolved in a mixed solvent of 0.5 mL degassed acetone and 0.5 mL degassed methanol under an argon atmosphere. To this mixture was added 5.5 μL methanol solution of HBr (1.91 M, 0.0105 mmol) and the solution was stirred at ambient temperature for 30 min. Removing solvents provided Ru-**3b** as an orange-yellow viscous liquid, which was immediately used for enantioselective hydrogenation of MAA. The preceding Ru-**3b** catalyst (0.00313 mmol) and 0.34 mL MAA (3.13 mmol) were dissolved in 2 mL degassed methanol. This solution was transferred to a 60 mL stainless-steel autoclave under Ar, and H_2 was charged into the reactor and the pressure was allowed to reach 4.0 MPa. The reactor was heated to 60 °C simultaneously with stirring at 400 rpm. The reactor was kept at 60 °C for 20 h and cooled to room temperature, and the excess hydrogen was carefully vented. The reaction solution was transferred to a Schlenk flask under Ar and the methanol was evaporated under vacuum, and *n*-hexane (2 × 4 mL) was added to extract the product. The system was cooled to below 10 °C by ice water, the upper organic phase was submitted to GC through a liquid-solid phase separation for the analysis of conversion and enantioselectivity, while the catalyst phase solidified at the bottom was supplemented with fresh methanol and MAA before the next run.

2 NMR Spectra

2.1 ^{1}H NMR spectrum of **2a**

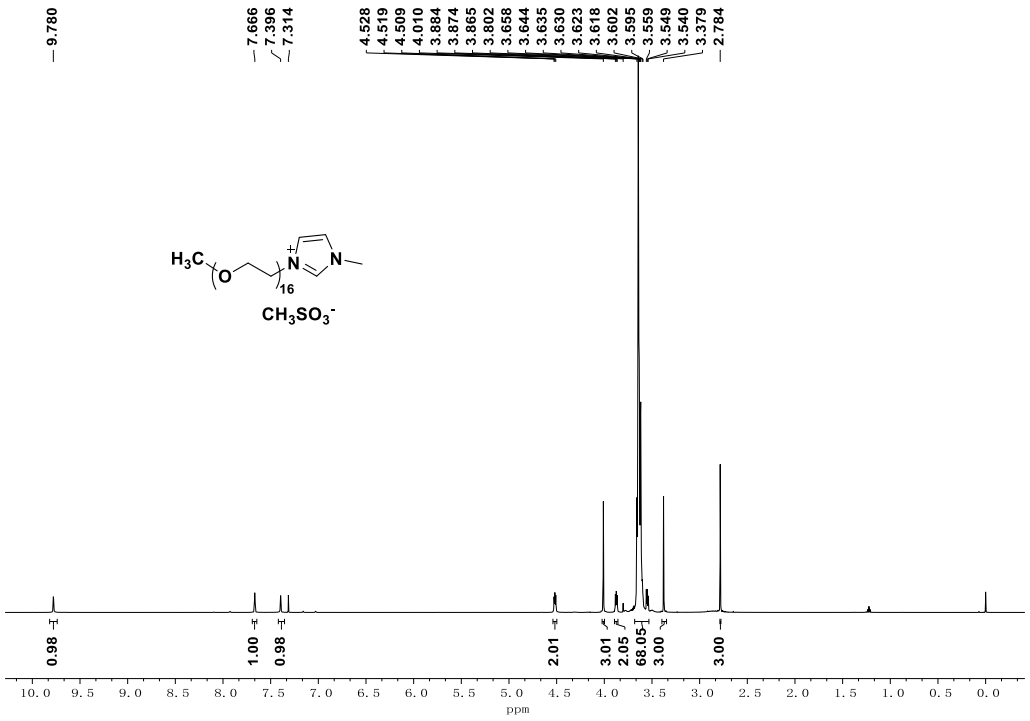

Figure S1. ^{1}H NMR spectrum of [Me(EO)$_{16}$MIM][OMs] (**2a**) (500.0 MHz, $CDCl_3$)

2.2 ^{13}C NMR spectrum of **2a**

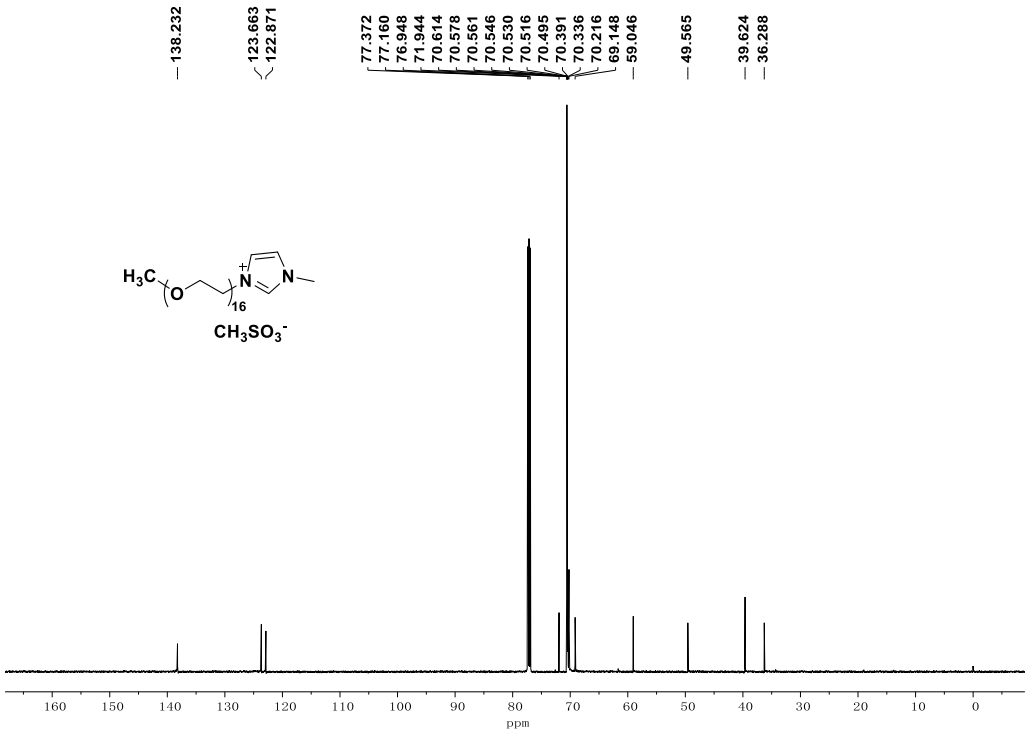

Figure S2. ^{13}C NMR spectrum of [Me(EO)$_{16}$MIM][OMs] (**2a**) (150.9 MHz, $CDCl_3$)

2.3 ^{1}H NMR spectrum of **2b**

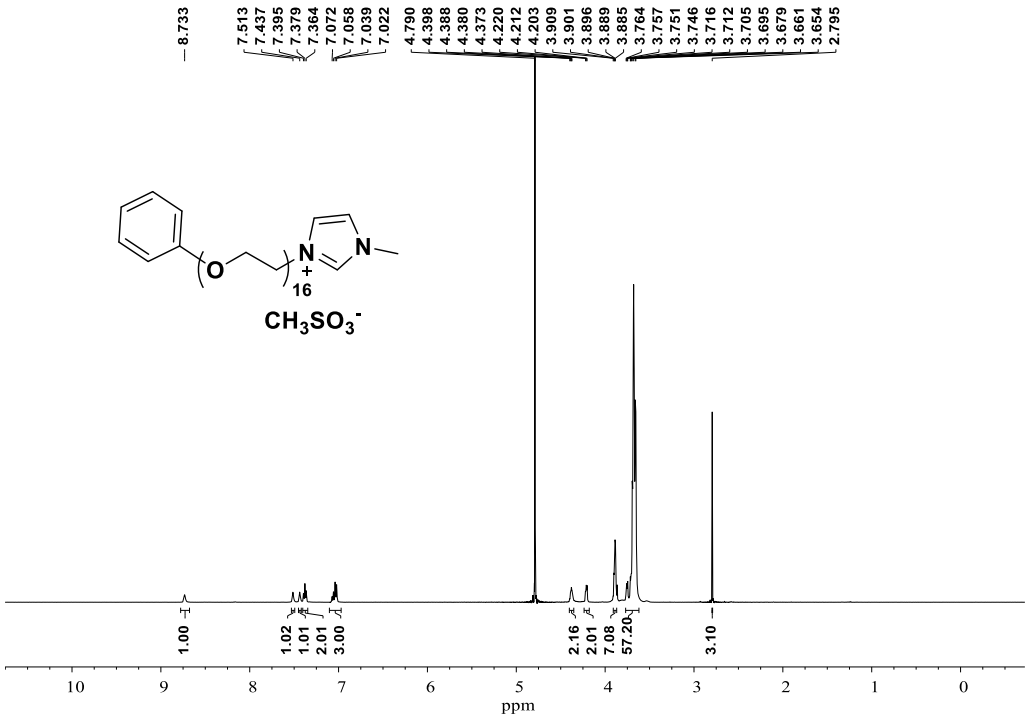

Figure S3. ^{1}H NMR spectrum of [Ph(EO)$_{16}$MIM][OMs] (**2b**) (500.0 MHz, D_2O)

2.4 ^{13}C NMR spectrum of **2b**

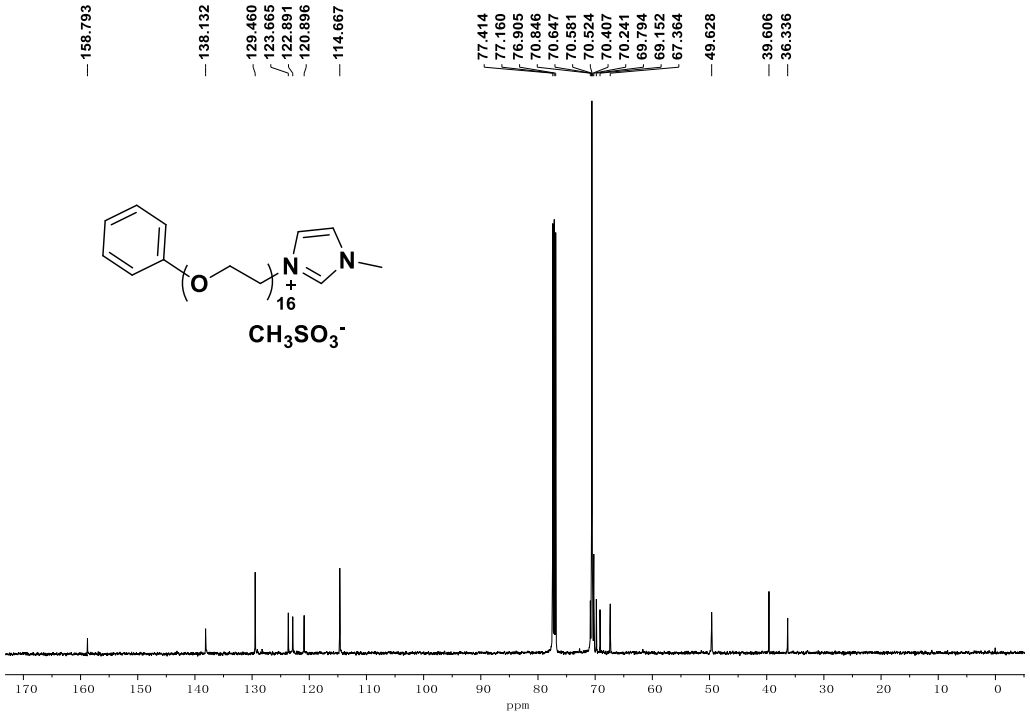

Figure S4. ^{13}C NMR spectrum of the [Ph(EO)$_{16}$MIM][OMs] (**2b**) (125.7 MHz, $CDCl_3$)

2.5 ^{1}H NMR spectrum of $Ph(CH_2)_2OMs$

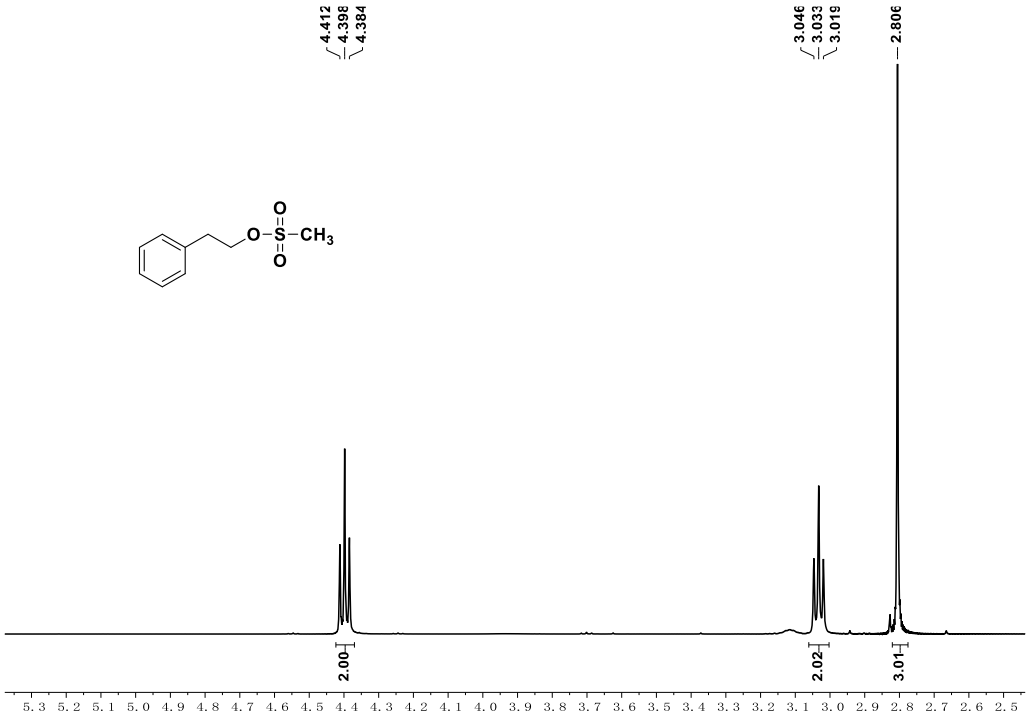

Figure S5. ^{1}H NMR spectrum of $Ph(CH_2)_2OMs$ (500.0 MHz, $CDCl_3$)

2.6 ^{1}H NMR spectrum of **6**

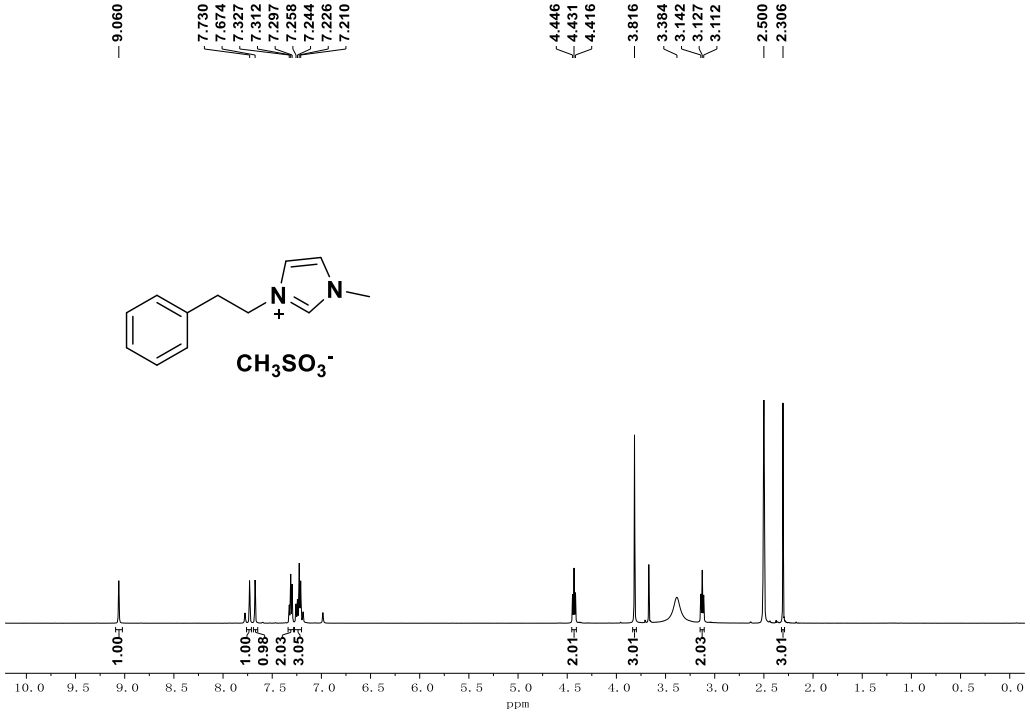

Figure S6. ^{1}H NMR spectrum of $[Ph(CH_2)_2MIM][OMs]$ (500.0 MHz, DMSO-d_6)

2.7 ^{13}C NMR spectrum of **6**

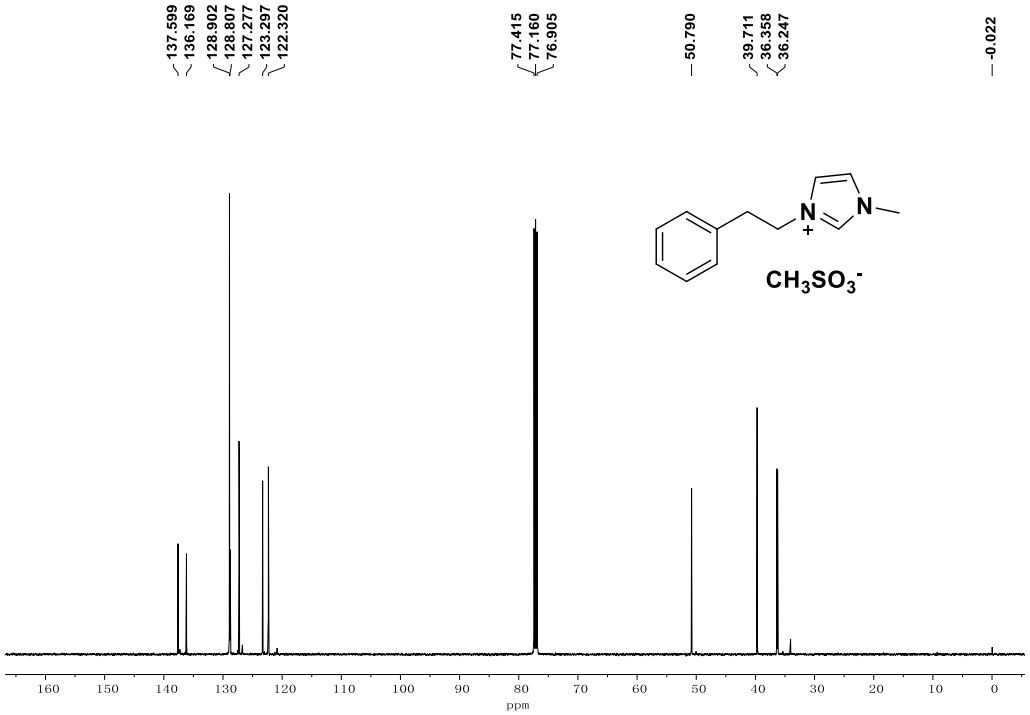

Figure S7. ^{13}C NMR spectrum of [Ph$(CH_2)_2$MIM][OMs] (125.7 MHz, $CDCl_3$)

2.8 ^{1}H NMR spectrum of **3a**

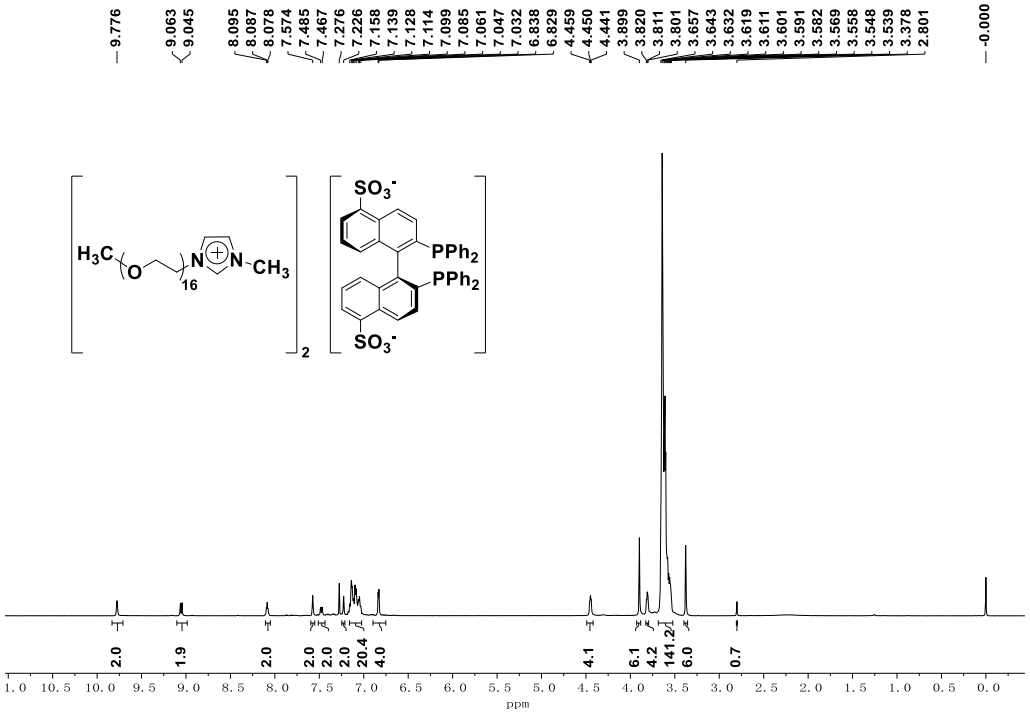

Figure S8. ^{1}H NMR spectrum of [Me$(EO)_{16}$MIM]$_2$[(*S*)-BINAP-$(SO_3)_2$] (**3a**) (500.0 MHz, $CDCl_3$)

2.9 ^{13}C NMR spectrum of **3a**

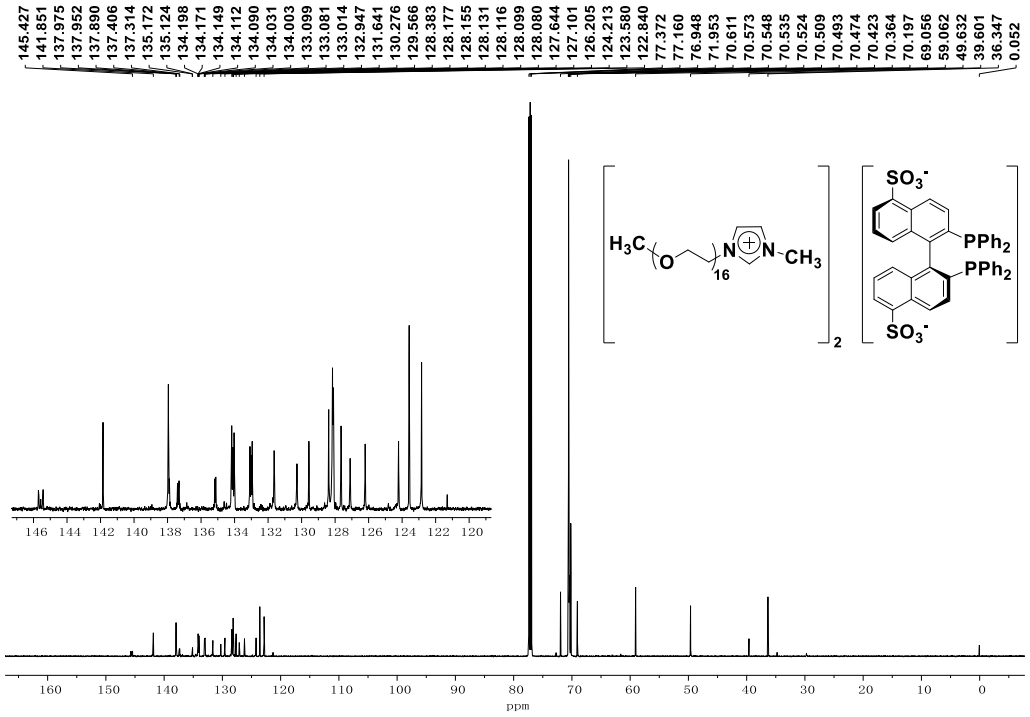

Figure S9. ^{13}C NMR spectrum of $[Me(EO)_{16}MIM]_2[(S)\text{-BINAP-}(SO_3)_2]$ (**3a**) (150.9 MHz, $CDCl_3$)

2.10 ^{31}P NMR spectrum of **3a**

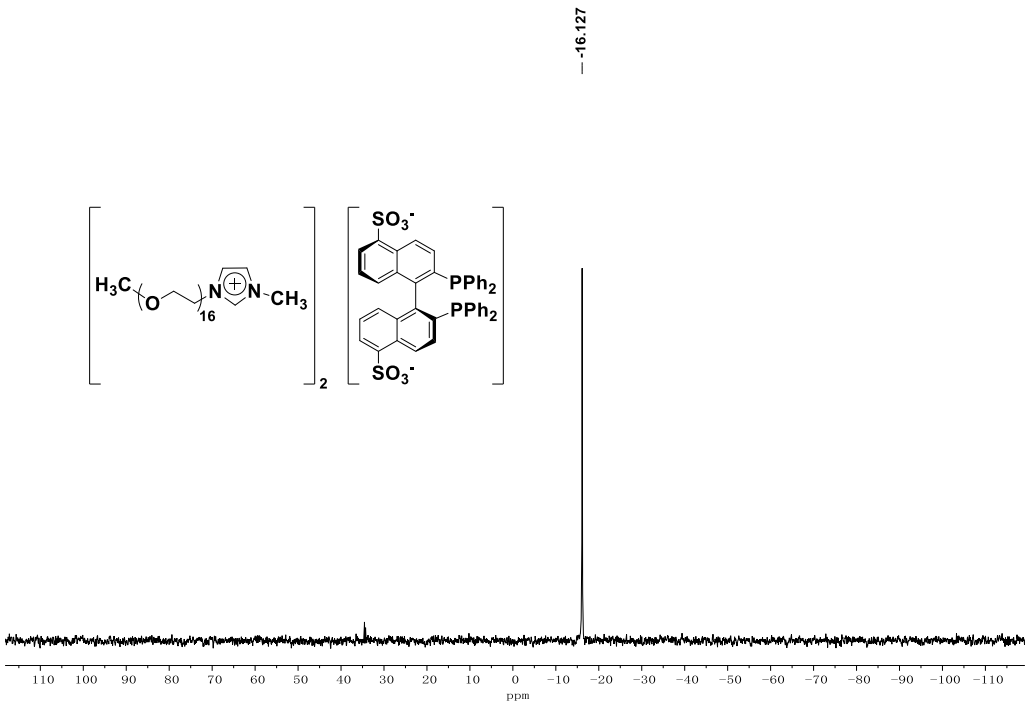

Figure S10. ^{31}P NMR spectrum of $[Me(EO)_{16}MIM]_2[(S)\text{-BINAP-}(SO_3)_2]$ (**3a**) (202.4 MHz, D_2O)

2.11 ^{1}H NMR spectrum of **3b**

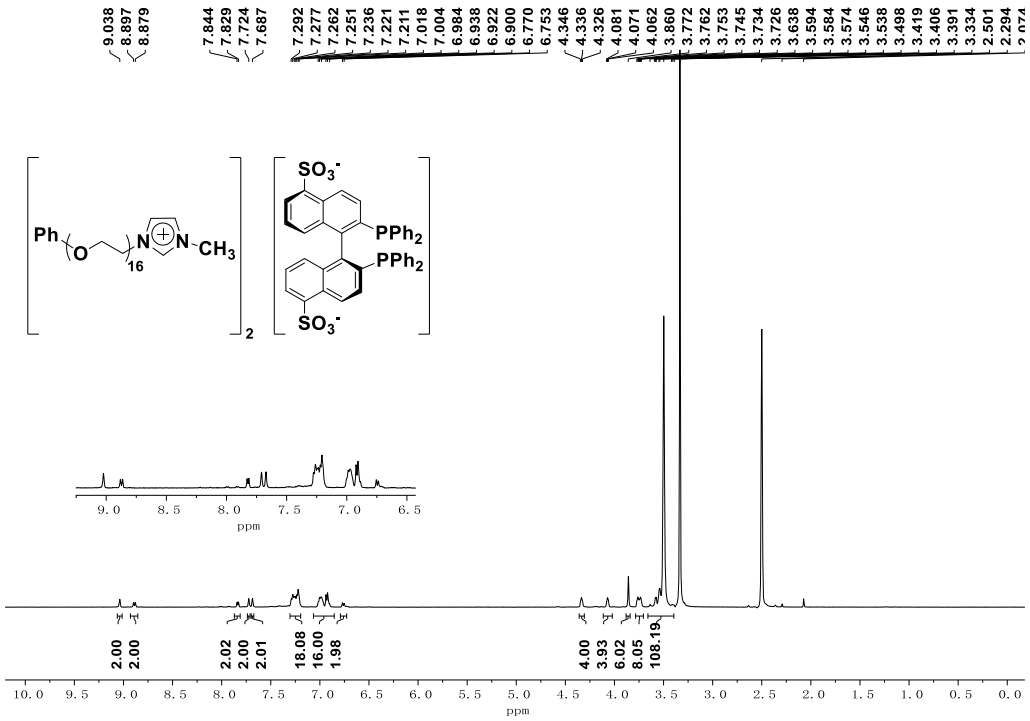

Figure S11. ^{1}H NMR spectrum of [Ph(EO)$_{16}$MIM]$_2$[(*S*)-BINAP-(SO$_3$)$_2$] (**3b**) (500.0 MHz, DMSO-d$_6$)

2.12 ^{13}C NMR spectrum of **3b**

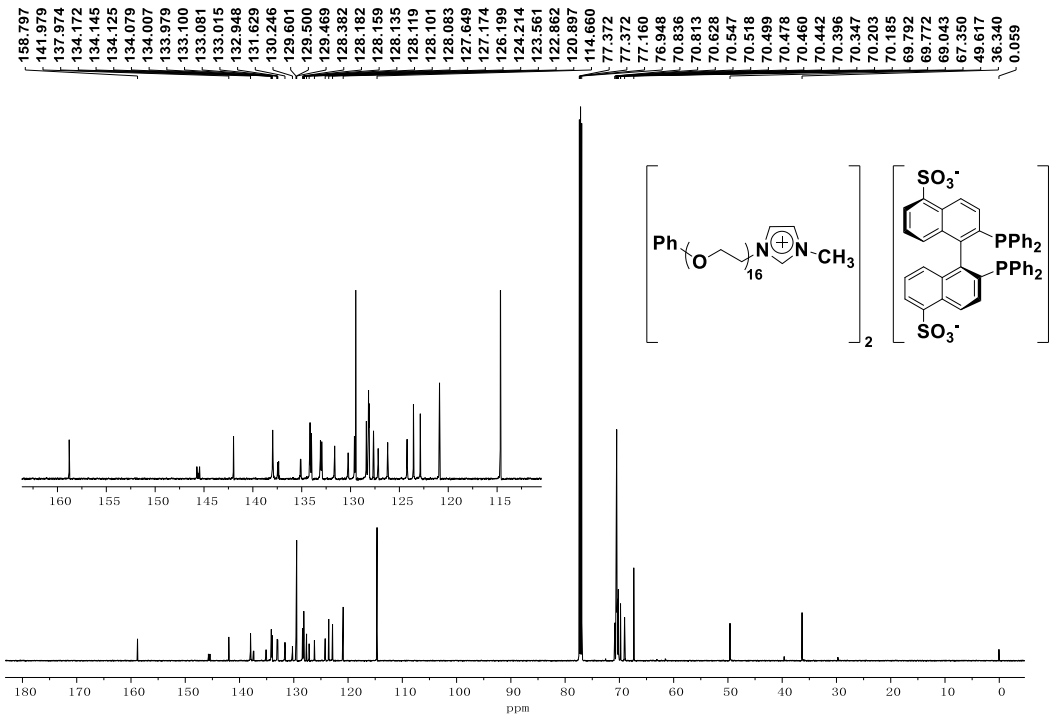

Figure S12. ^{13}C NMR spectrum of [Ph(EO)$_{16}$MIM]$_2$[(*S*)-BINAP-(SO$_3$)$_2$] (**3b**) (150.9 MHz, CDCl$_3$)

2.13 ^{31}P NMR spectrum of **3b**

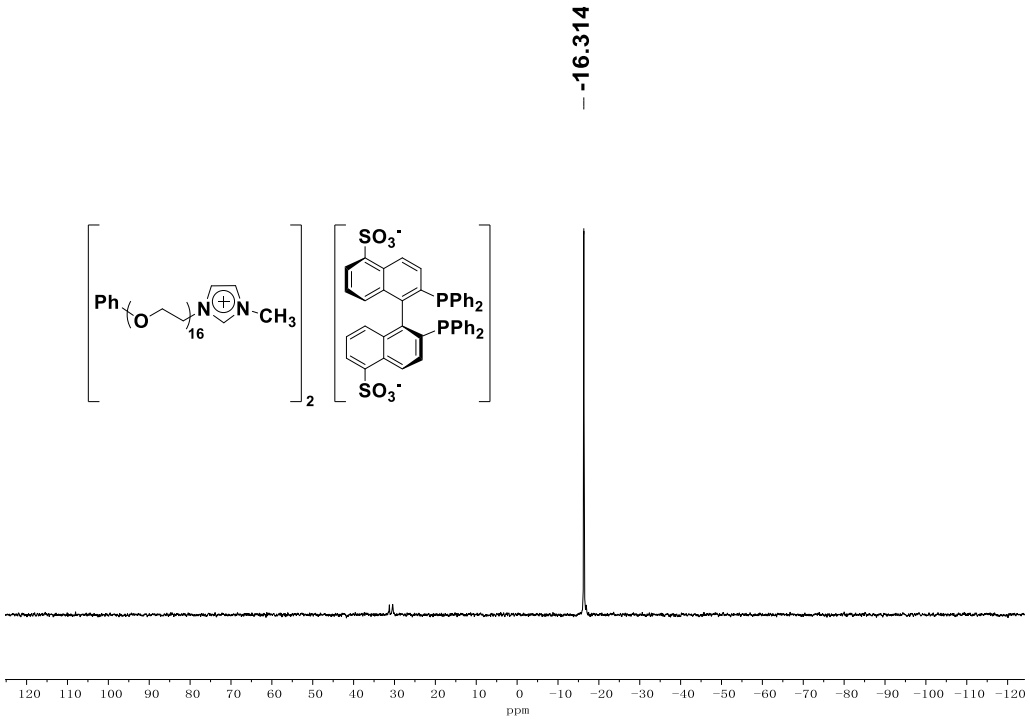

Figure S13. ^{31}P NMR spectrum of [Ph(EO)$_{16}$MIM]$_2$[(*S*)-BINAP-(SO$_3$)$_2$] (**3b**) (202.4 MHz, CDCl$_3$)

2.14 ^{1}H NMR spectrum of **7**

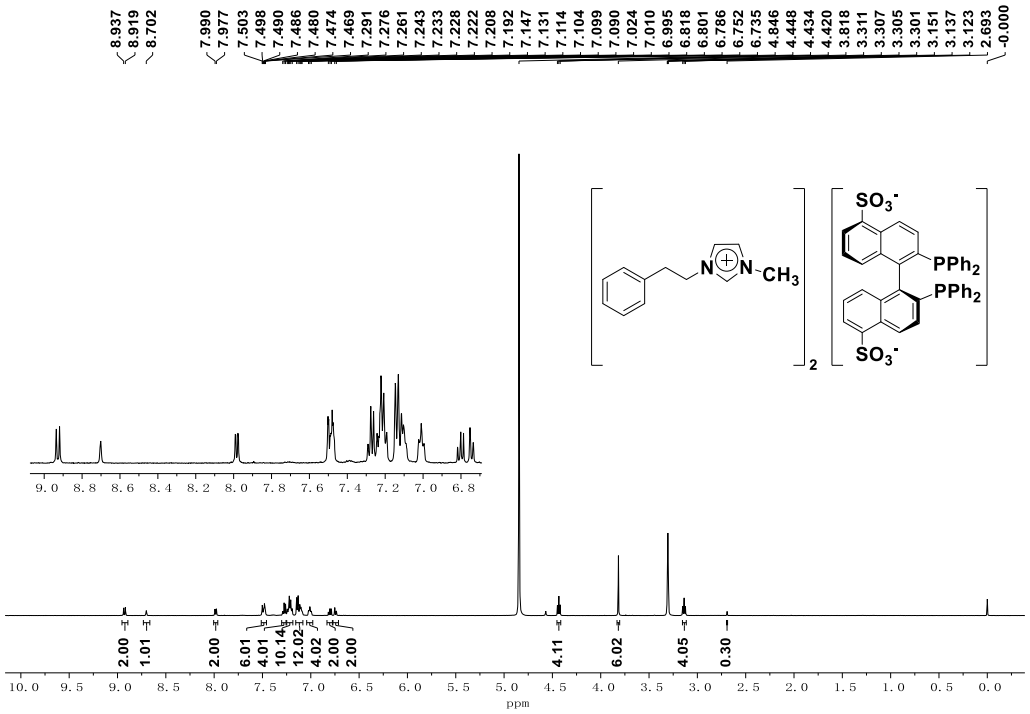

Figure S14. ^{1}H NMRspectra of [Ph(CH$_2$)$_2$MIM]$_2$[(*S*)-BINAP-(SO$_3$)$_2$] (**7**) (500.0 MHz, CD$_3$OD)

2.15 ^{13}C NMR spectrum of **7**

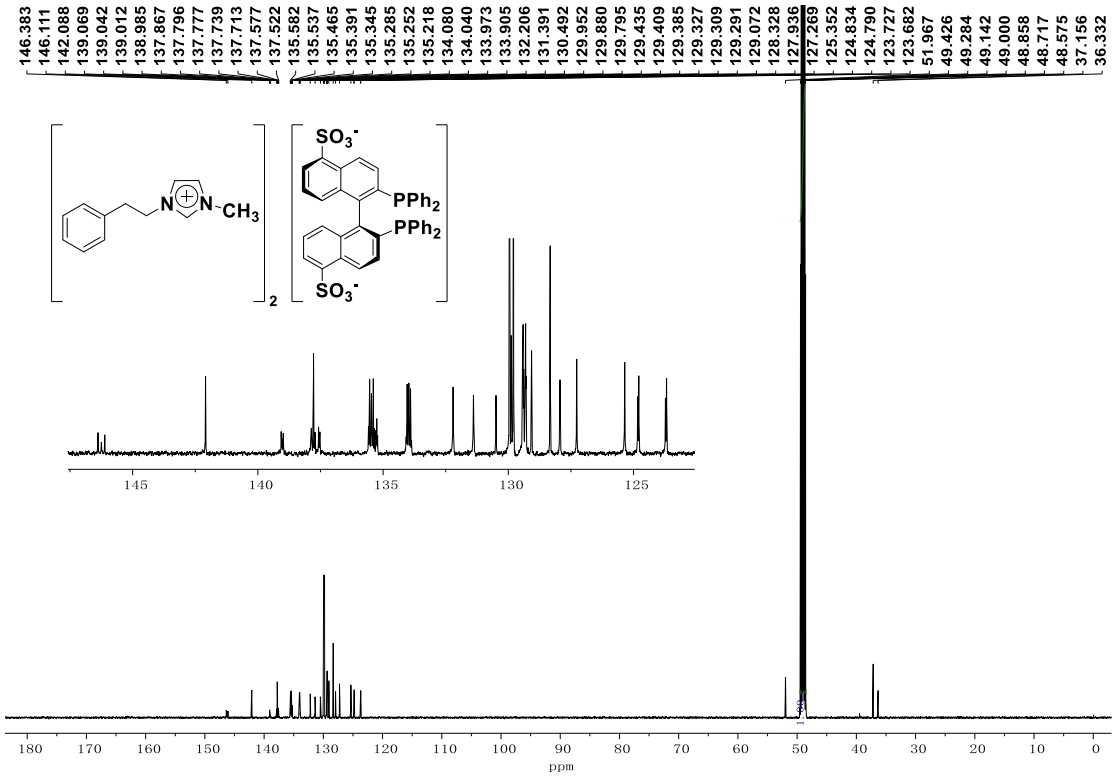

Figure S15. ^{13}C NMR spectrum of [Ph(CH$_2$)$_2$MIM]$_2$[(*S*)-BINAP-(SO$_3$)$_2$] (**7**) (150.9 MHz, CD$_3$OD)

2.16 ^{31}P NMR spectrum of **7**

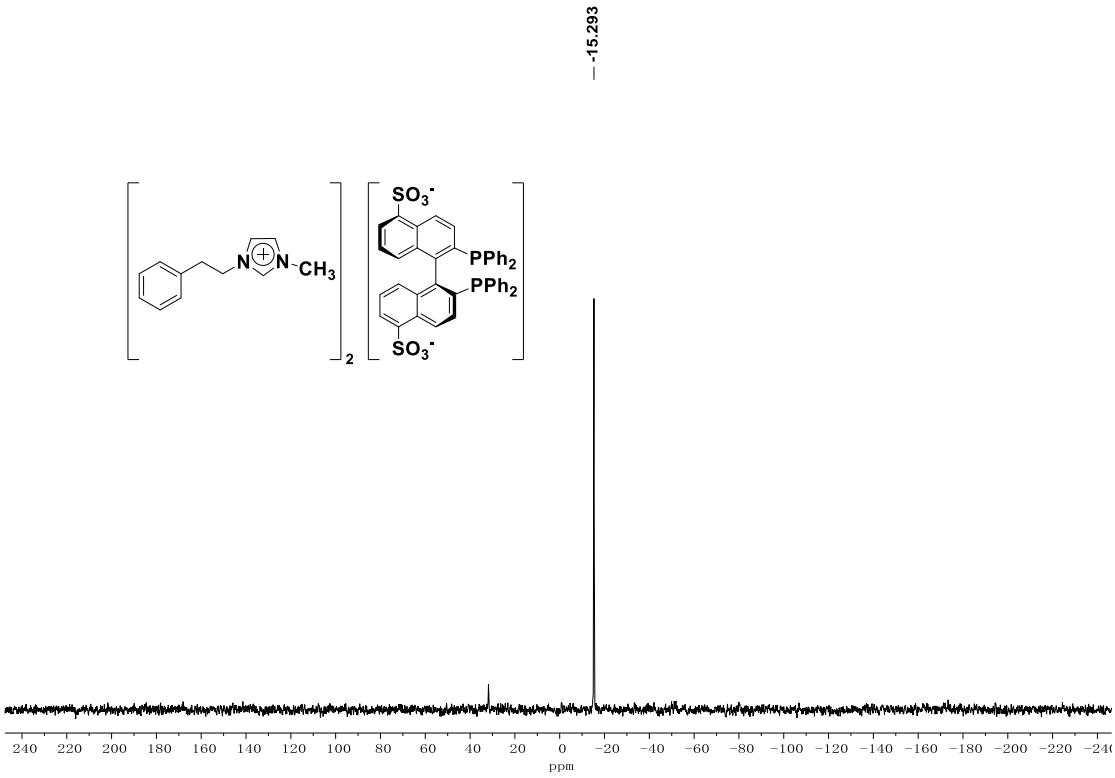

Figure S16. ^{31}P NMR spectrum of [Ph(CH$_2$)$_2$MIM]$_2$[(*S*)-BINAP-(SO$_3$)$_2$] (**7**) (202.4 MHz, CD$_3$OD)

2.17 ^{1}H NMR spectrum of methyl (*S*)-3-hydroxybutyrate (**5a**)

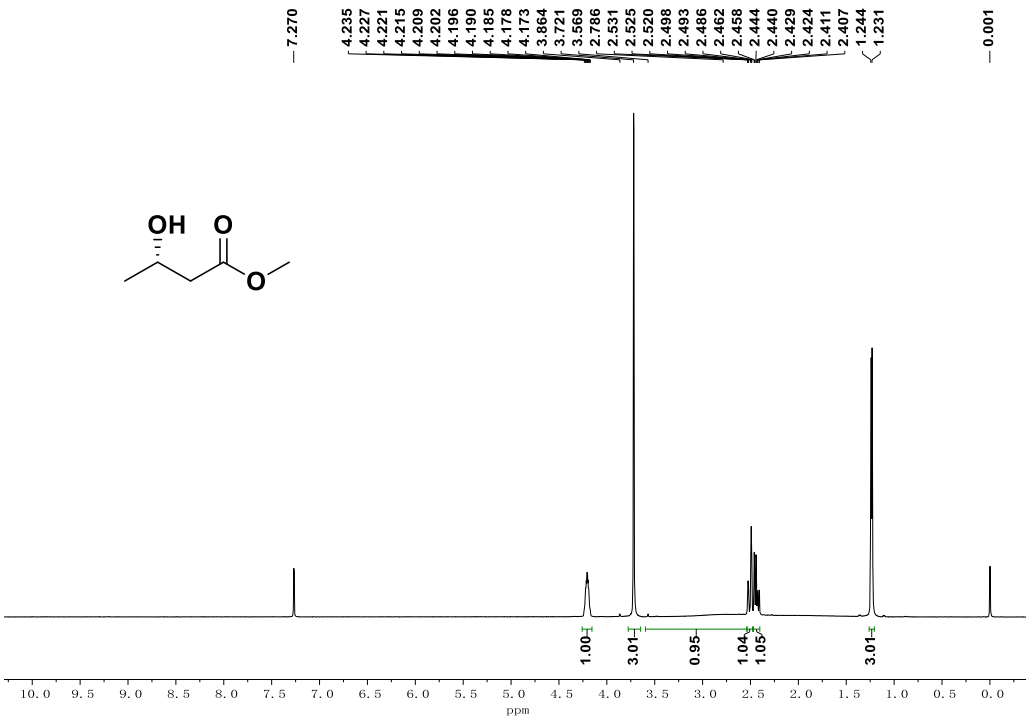

Figure S17. ^{1}H NMR spectrum of methyl (*S*)-3-hydroxybutyrate (**5a**) (500.0 MHz, $CDCl_3$)

2.18 ^{1}H NMR spectrum of ethyl (*S*)-3-hydroxybutyrate (**5b**)

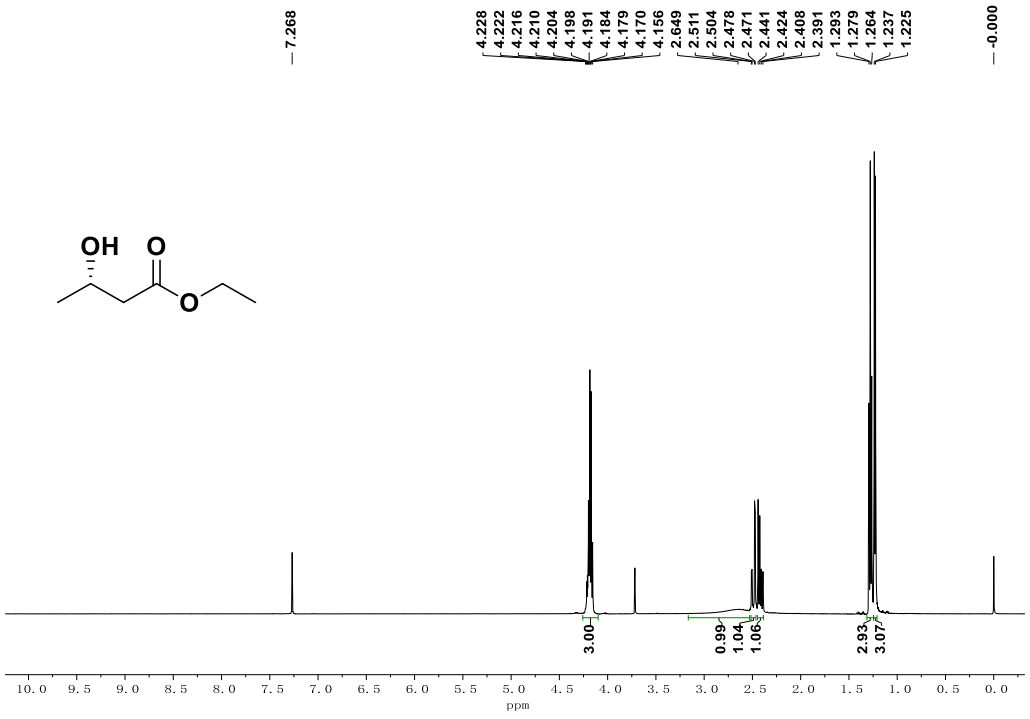

Figure S18. ^{1}H NMR spectrum of ethyl (*S*)-3-hydroxybutyrate (**5b**) (500.0 MHz, $CDCl_3$)

2.19 ^{1}H NMR spectrum of methyl (*S*)-3-hydroxyvalerate (**5c**)

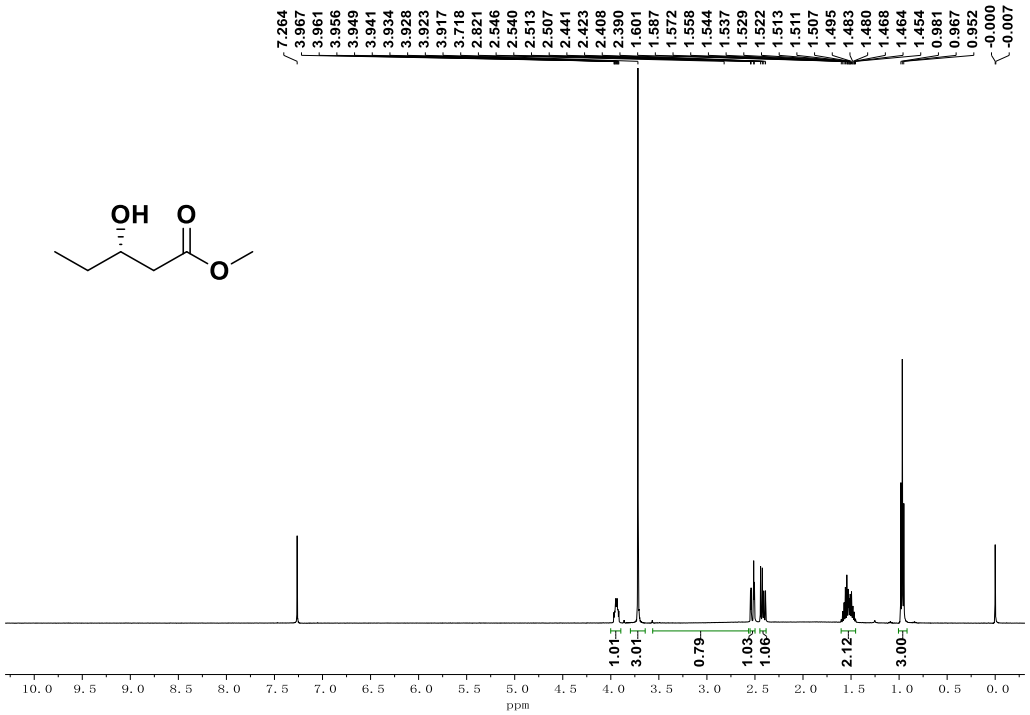

Figure S19. ^{1}H NMR spectrum of methyl (*S*)-3-hydroxyvalerate (**5c**) (500.0 MHz, $CDCl_3$)

2.20 ^{1}H NMR spectrum of isopropyl (*S*)-3-hydroxybutyrate (**5d**)

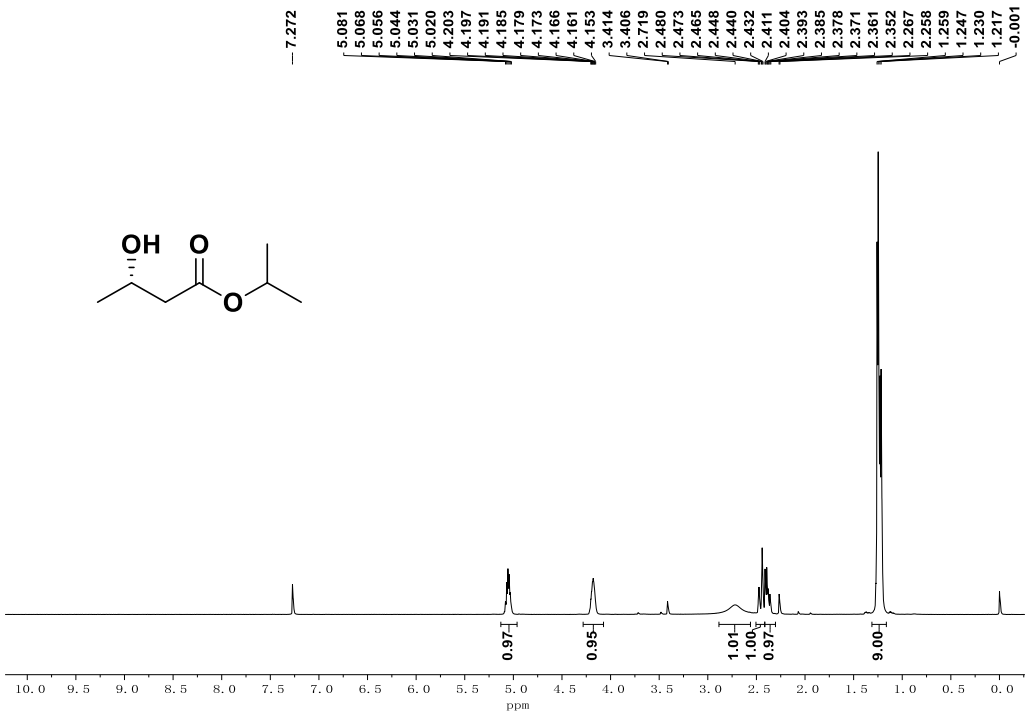

Figure S20. ^{1}H NMR spectrum of isopropyl (*S*)-3-hydroxybutyrate (**5d**) (500.0 MHz, $CDCl_3$)

2.21 ^{1}H NMR spectrum of tert-butyl (*S*)-3-hydroxybutyrate (**5e**)

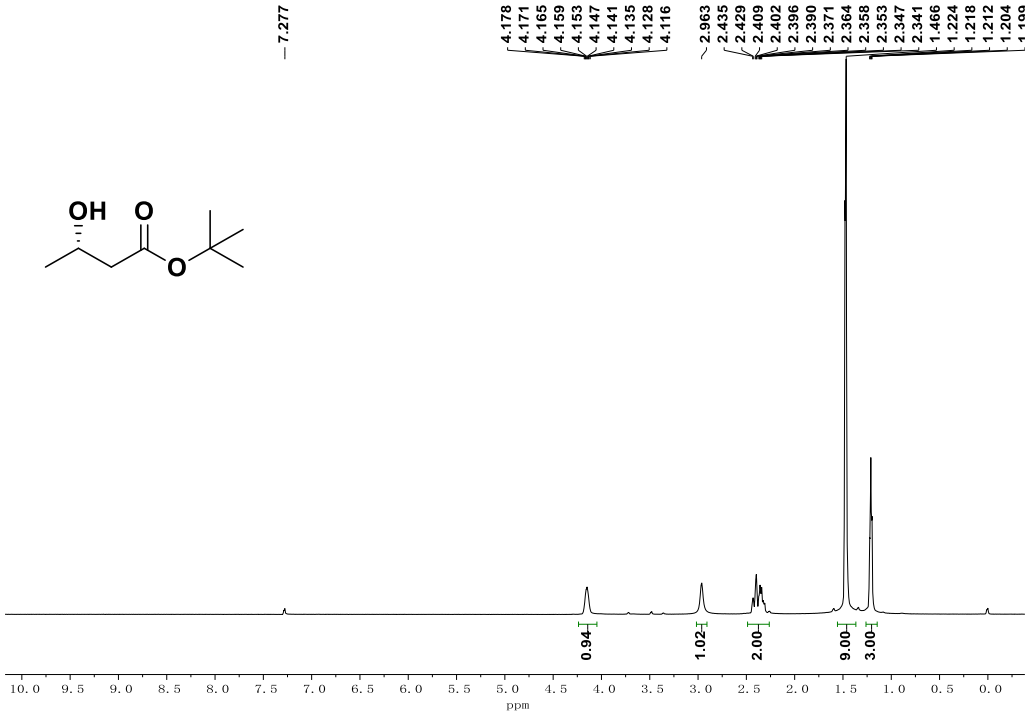

Figure S21. ^{1}H NMR spectrum of tert-butyl (*S*)-3-hydroxybutyrate (**5e**) (500.0 MHz, $CDCl_3$)

2.22 ^{1}H NMR spectrum of methyl (*S*)-2,2-dimethyl-3-hydroxybutyrate (**5f**)

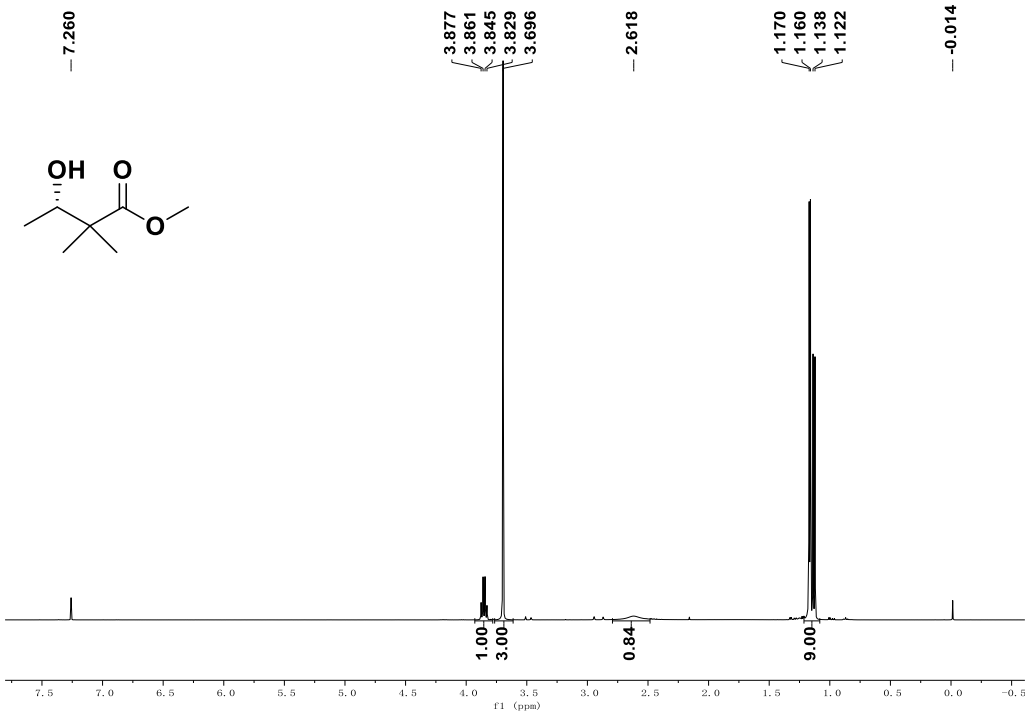

Figure S22. ^{1}H NMR spectrum of methyl (*S*)-2,2-dimethyl-3-hydroxybutyrate (**5f**) (500 MHz, $CDCl_3$)

2.23 ^{1}H NMR spectrum of methyl (*R*)-4-chloro-3-hydroxybutyrate (**5g**)

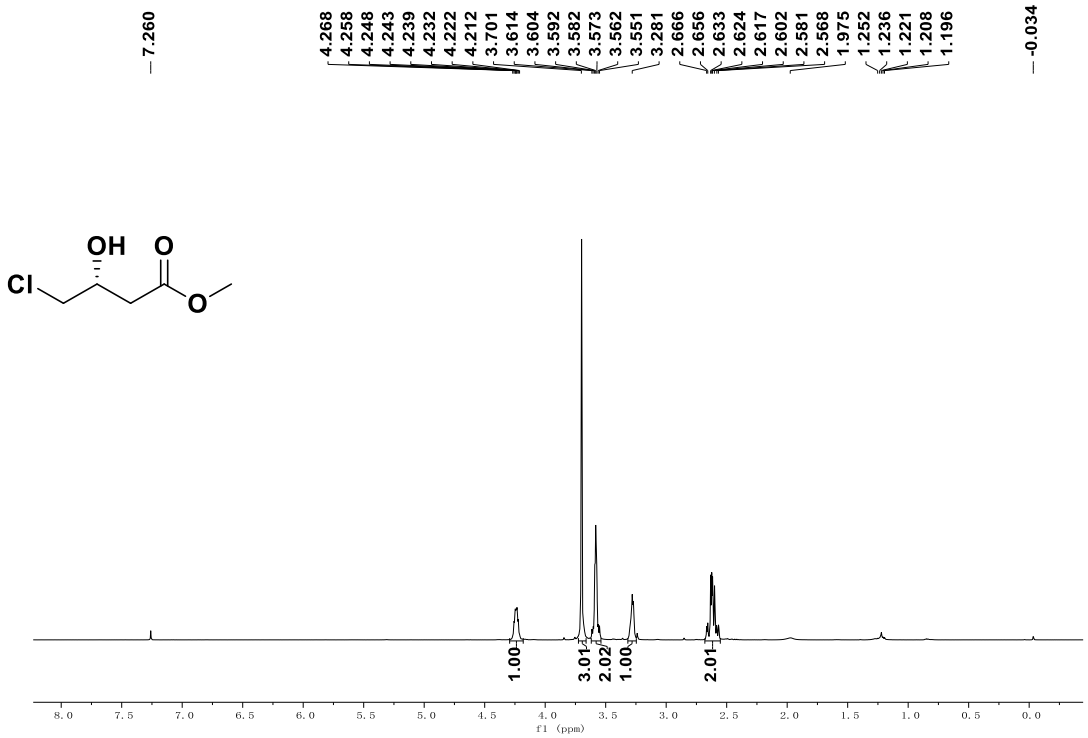

Figure S23. ^{1}H NMR spectrum of methyl (*R*)-4-chloro-3-hydroxybutyrate (**5g**) (500 MHz, $CDCl_3$)

2.24 ^{1}H NMR spectrum of ethyl (*R*)-4,4,4-trifluoro-3-hydroxybutyrate (**5h**)

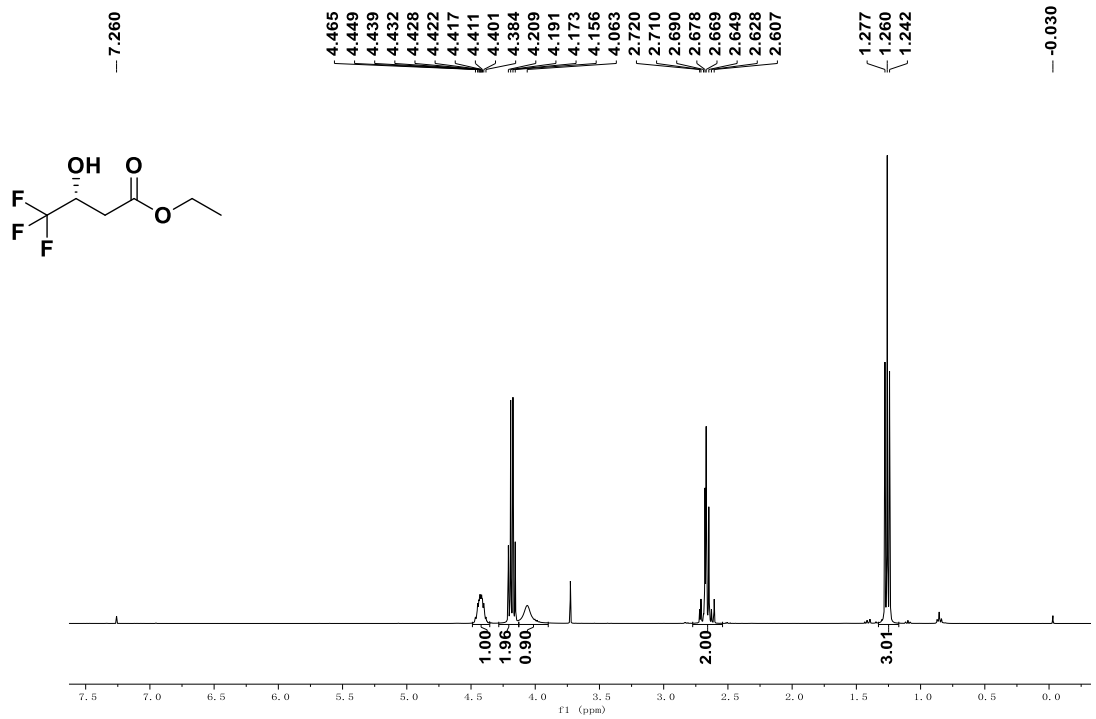

Figure S24. ^{1}H NMR spectrum of ethyl (*R*)-4,4,4-trifluoro-3-hydroxybutyrate (**5h**) (400 MHz, $CDCl_3$)

2.25 ^{1}H NMR spectrum of ethyl (*R*)-3-hydroxy-3-phenylpropanoate (**5i**)

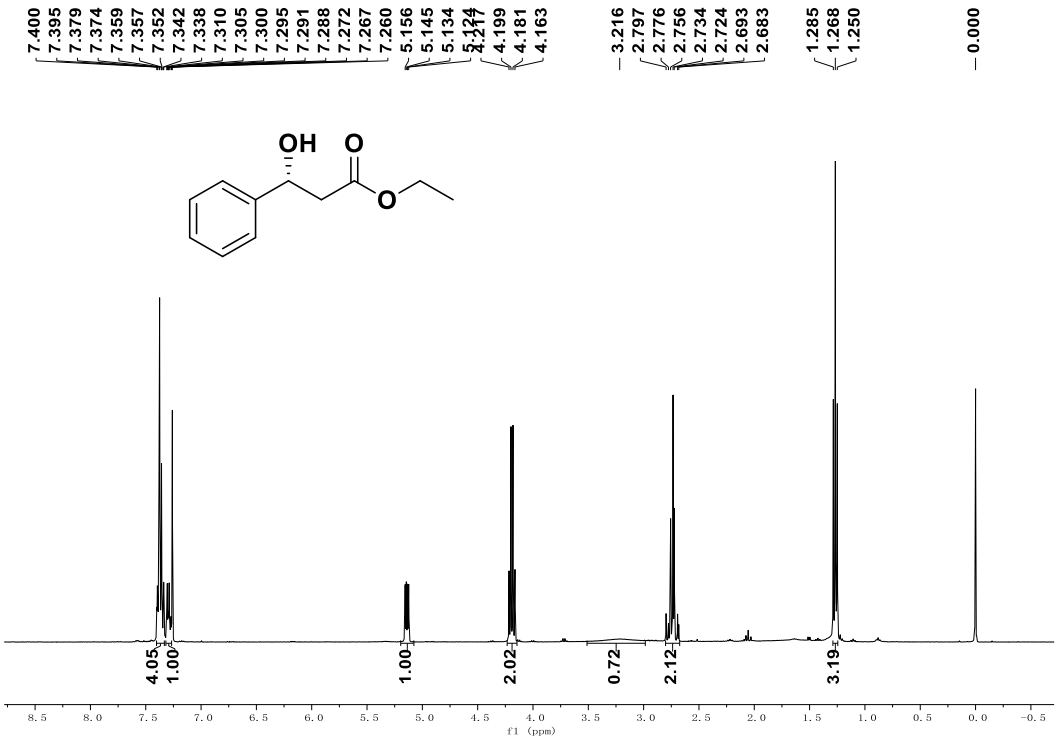

Figure S25. ^{1}H NMR spectrum of ethyl (*R*)-3-hydroxy-3-phenylpropanoate (**5i**) (500 MHz, $CDCl_3$)

2.26 ^{1}H NMR spectrum of ethyl (*R*)-3-methoxy-3-(4'-methoxyphenyl) propanoate (**5j**)

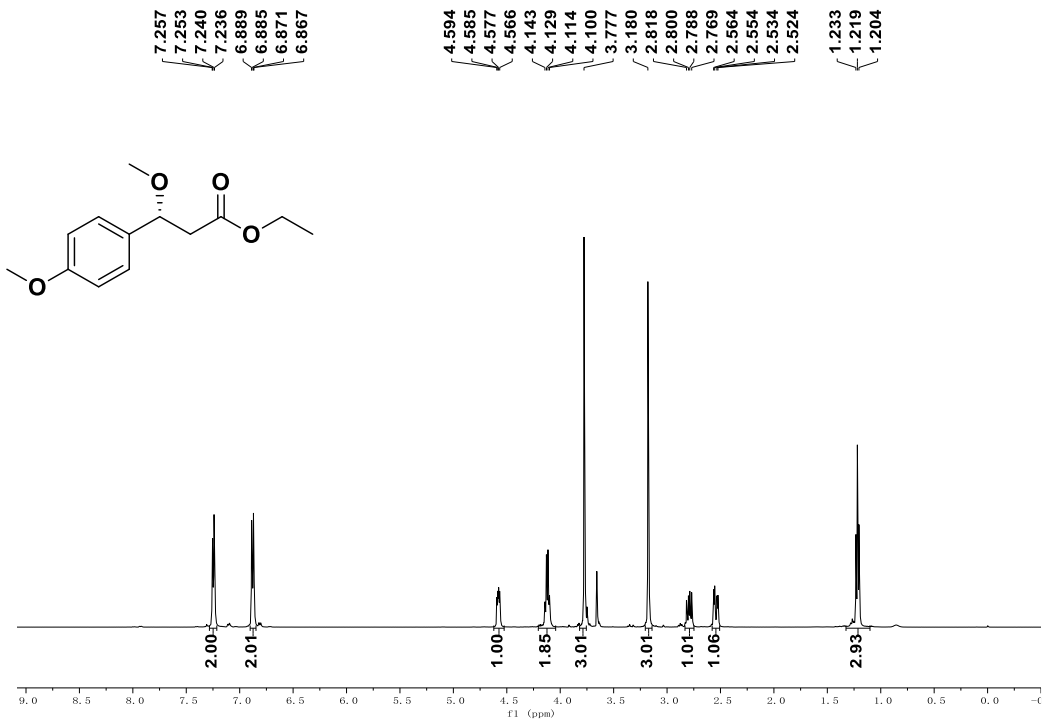

Figure S26. ^{1}H NMR spectrum of ethyl (*R*)-3-methoxy-3-(4'-methoxyphenyl) propanoate (**5j**) (500 MHz, $CDCl_3$)

2.27 ^{13}C NMR spectrum of ethyl (*R*)-3-methoxy-3-(4'-methoxyphenyl) propanoate (**5j**)

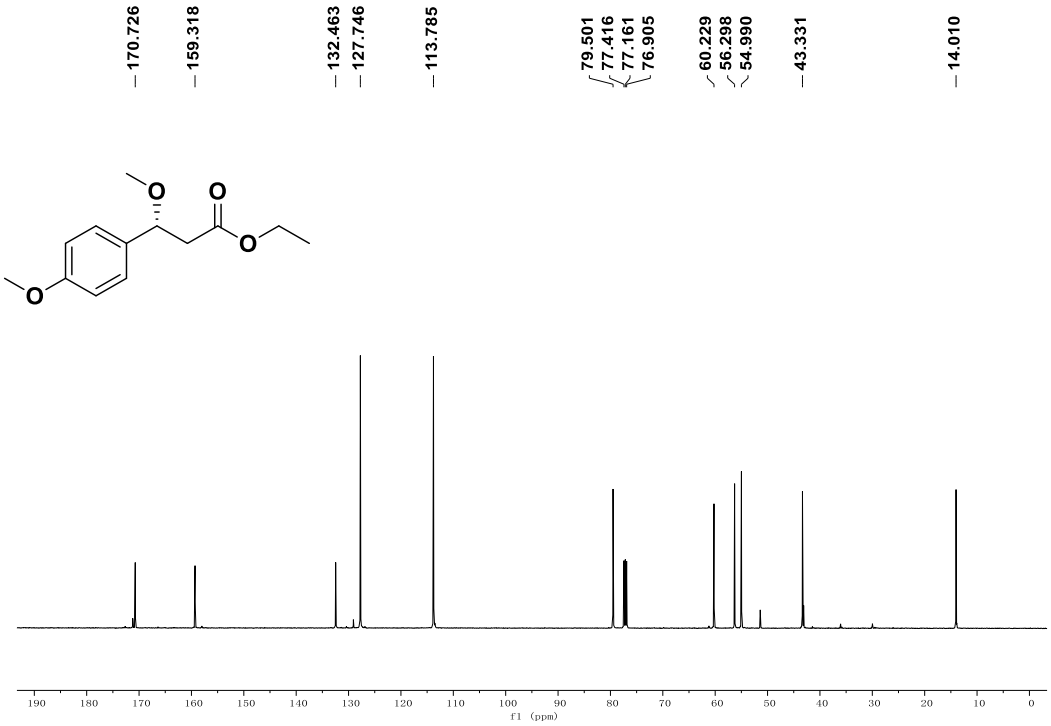

Figure S27. ^{13}C NMR spectrum of ethyl (*R*)-3-methoxy-3-(4'-methoxyphenyl) propanoate (**5j**) (500 MHz, $CDCl_3$)

2.28 2D ^{1}H-^{1}H COSY NMR spectrum of **3a**

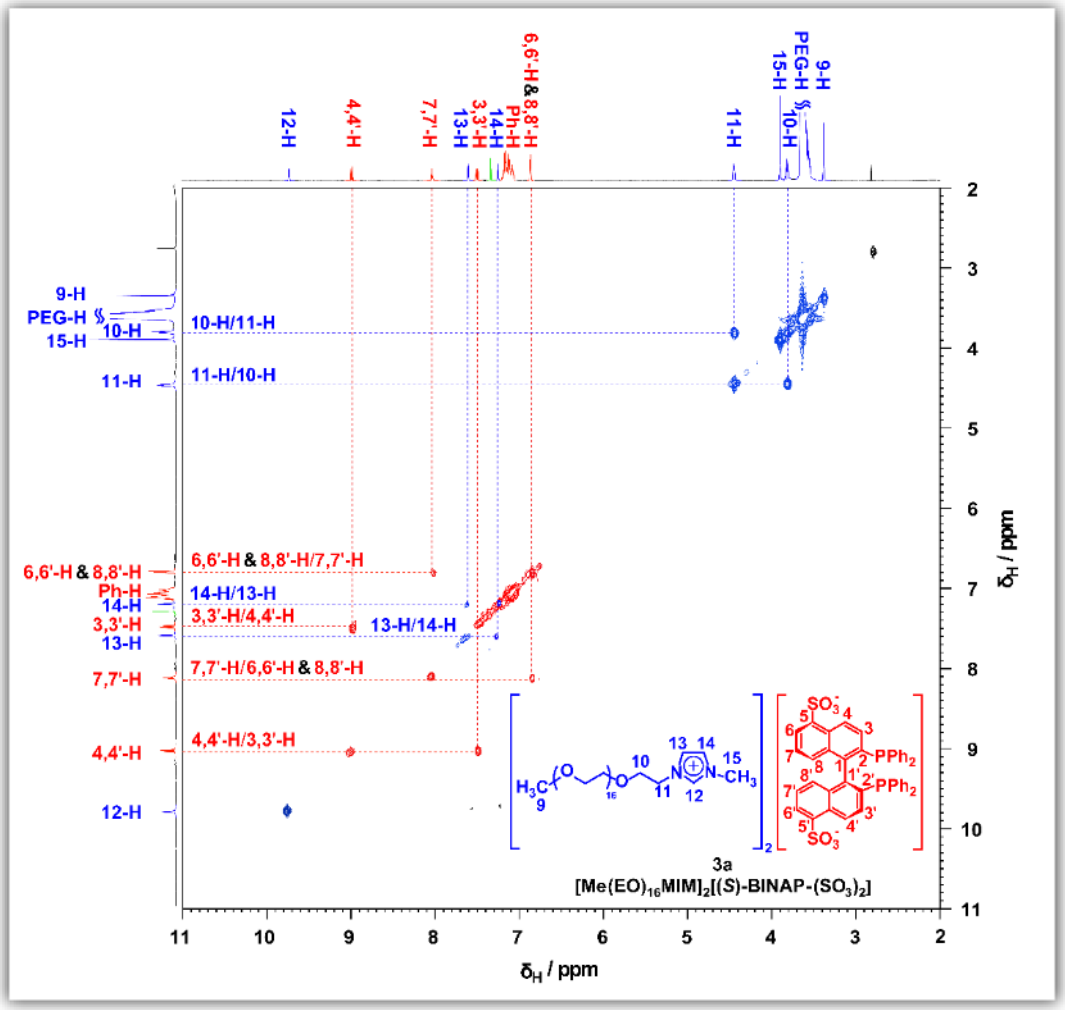

Figure S28. 2D ^{1}H-^{1}H COSY NMR spectrum of **3a**. The 2D ^{1}H-^{1}H COSY spectrum of **3a** clearly showed the chemical shifts of protons on $[Me(EO)_{16}MIM]^{+}$ cations (marked in blue) and $[(S)\text{-BINAP-}(SO_3)_2]^{2-}$ anion (marked in red). In particular, the resonance peaks at δ 9.06 (d, 2H, J = 9.0 Hz), 8.09 (t, 2H, J = 4.0 Hz), 7.48 (d, 2H, J = 9.0 Hz) and 6.84 (d, 4H, J = 4.0 Hz) can be assigned to protons of 4 (4')-, 7 (7')-, 3 (3')-, 6 (6') and 8 (8')-positions of the binaphthyl group by means of identification of the correlation peaks. According to the integral analysis of the proton signals on the polyether imidazolium cations and sulfonated BINAP anions, the molar ratio of $[Me(EO)_{16}MIM]^{+}$ cations to $[(S)\text{-BINAP-}(SO_3)_2]^{2-}$ anions was 2:1, confirming that the ion exchange was completed.

3 MS Spectra

3.1 Mass spectrum (ESI positive) of **2a**

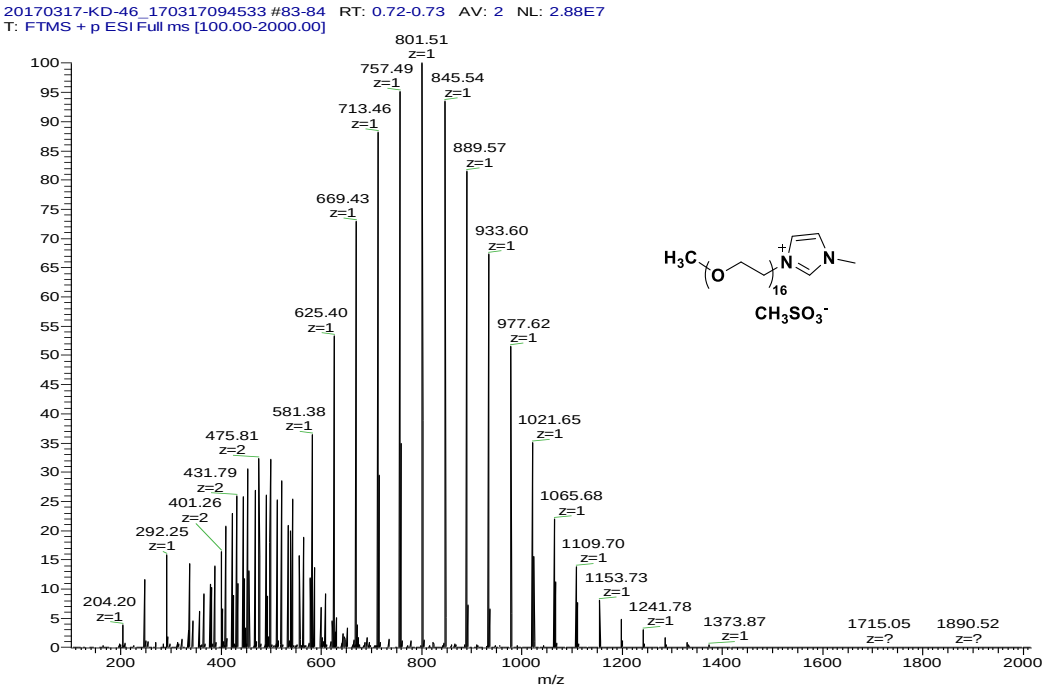

Figure S29. Mass spectrum (ESI positive) of [Me(EO)$_{16}$MIM][OMs] (**2a**)

3.2 Mass spectrum (ESI negative) of **2a**

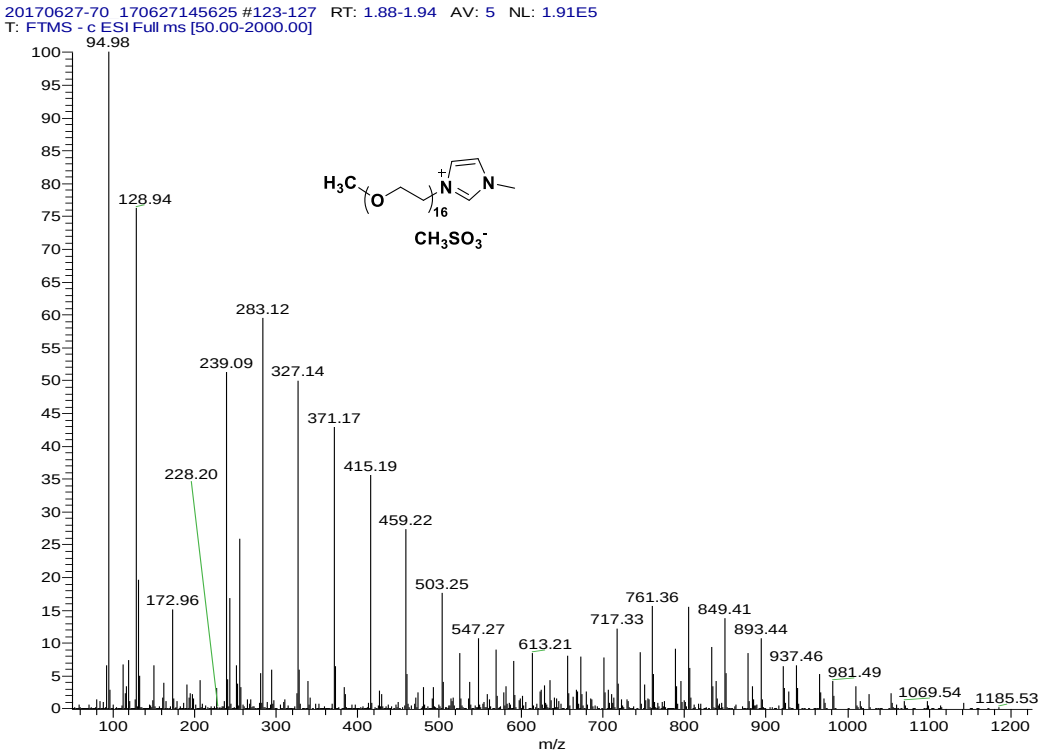

Figure S30. Mass spectrum (ESI negative) of [Me(EO)$_{16}$MIM][OMs] (**2a**)

3.3 Mass spectrum (ESI positive) of **2b**

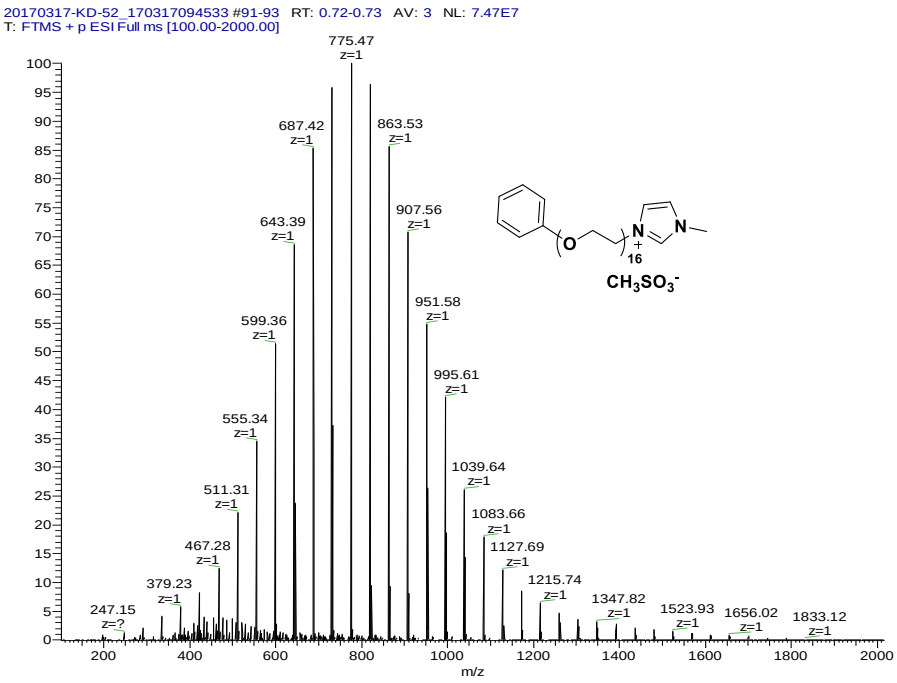

Figure S31. Mass spectrum (ESI positive) of [Ph(EO)$_{16}$MIM][OMs] (**2b**)

3.4 Mass spectrum (ESI negative) of **2b**

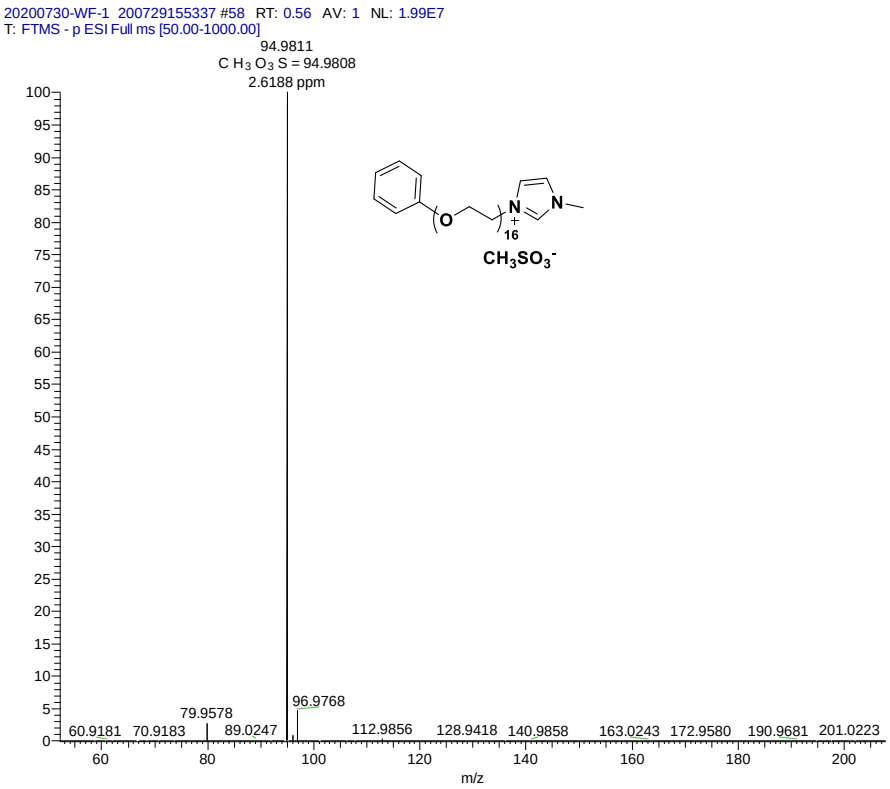

Figure S32. Mass spectrum (ESI negative) of [Ph(EO)$_{16}$MIM][OMs] (**2b**)

3.5 Mass spectrum (ESI positive) of **6**

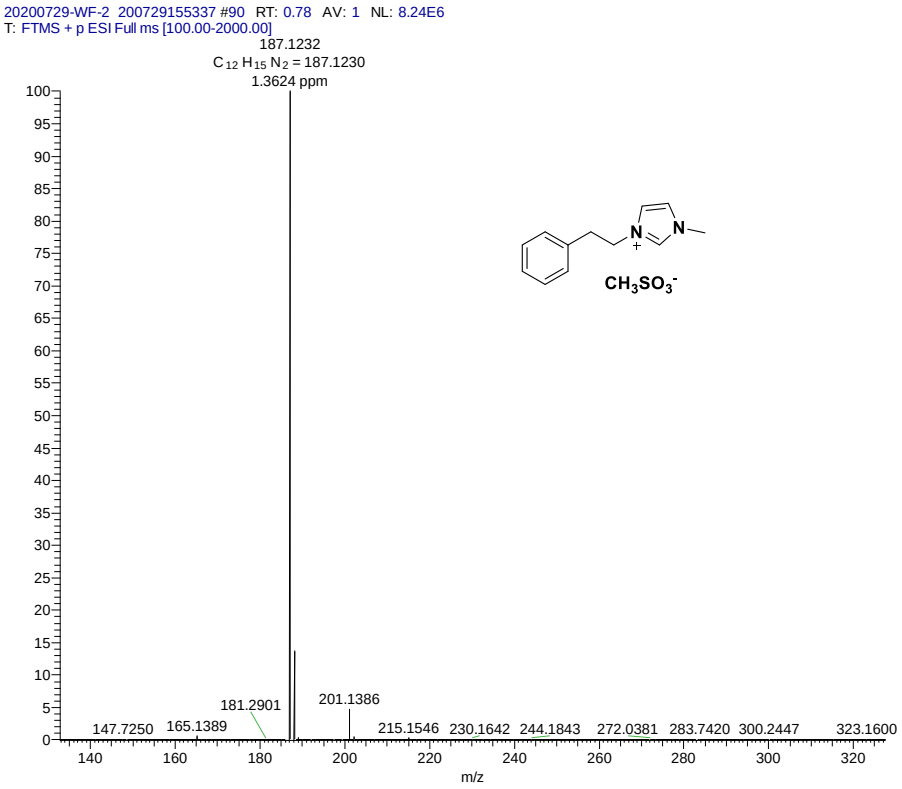

Figure S33. Mass spectrum (ESI positive) of [Ph(CH_2)$_2$MIM][OMs] (**6**)

3.6 Mass spectrum (ESI negative) of **6**

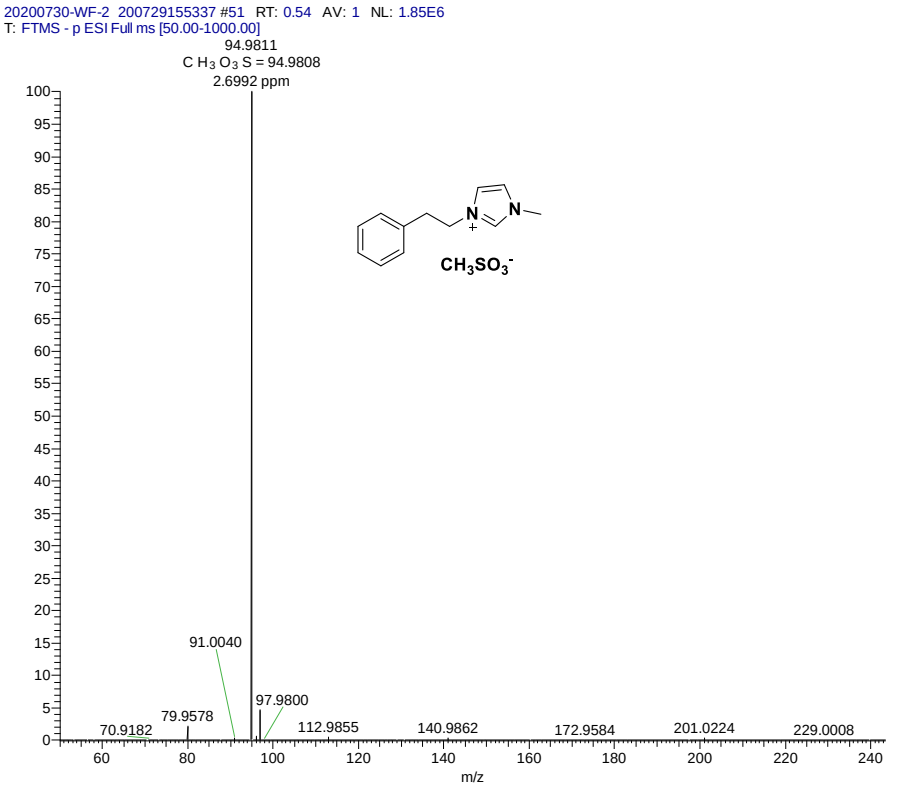

Figure S34. Mass spectrum (ESI negative) of [Ph(CH_2)$_2$MIM][OMs] (**6**)

3.7 Mass spectrum (ESI positive) of **3a**

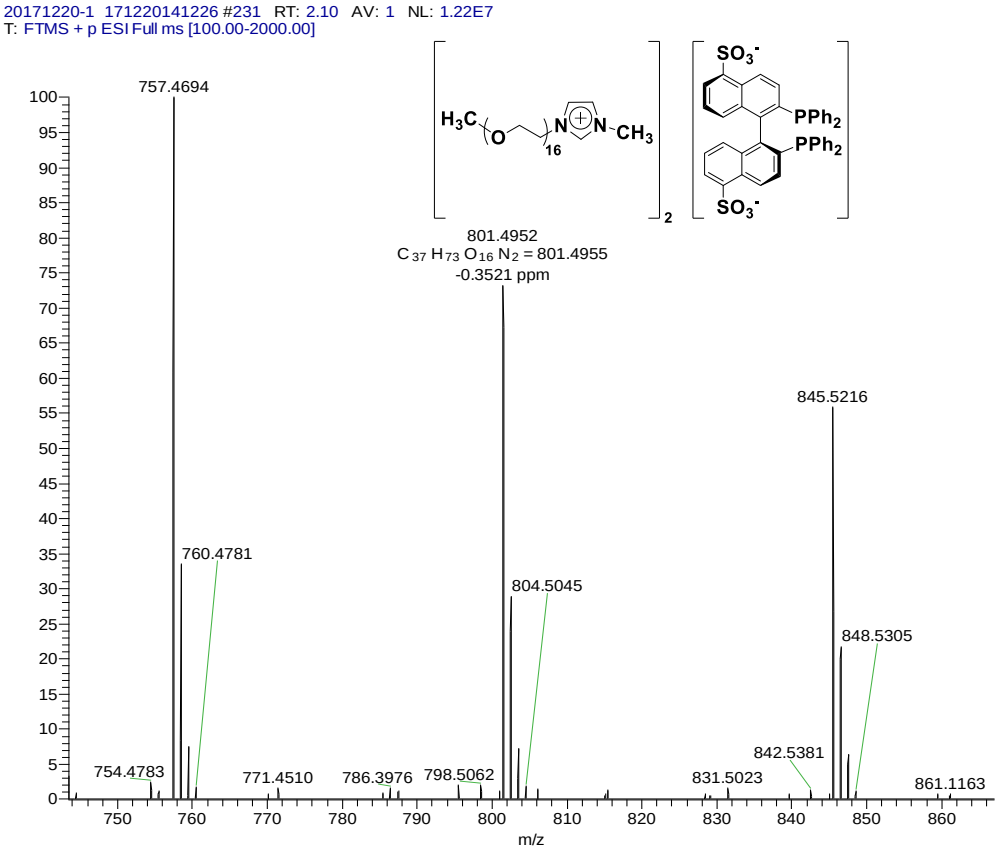

Figure S35. Mass spectrum (ESI positive) of $[Me(EO)_{16}MIM]_2[(S)\text{-BINAP-}(SO_3)_2]$ (**3a**)

3.8 Mass spectrum (ESI negative) of **3a**

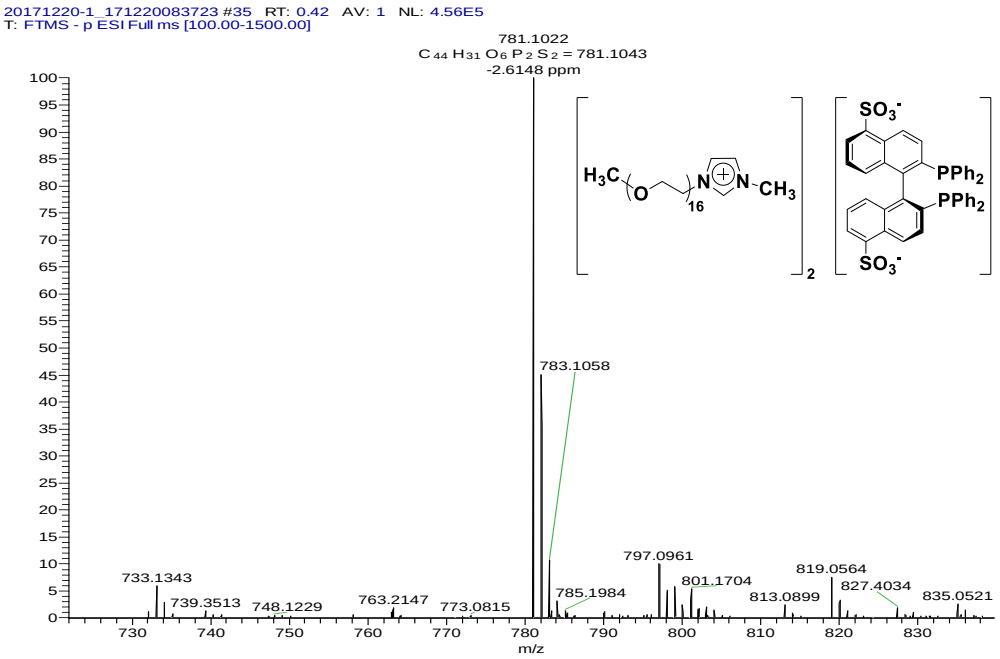

Figure S36. Mass spectrum (ESI negative) of $[Me(EO)_{16}MIM]_2[(S)\text{-BINAP-}(SO_3)_2]$ (**3a**)

3.9 Mass spectrum (ESI positive) of **3b**

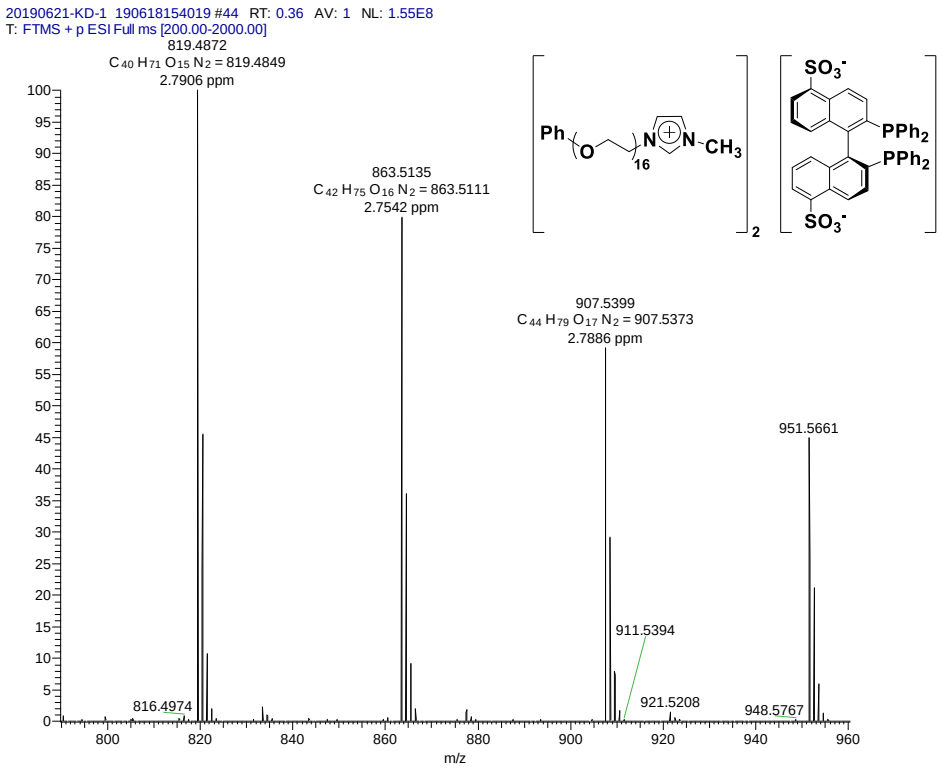

Figure S37. Mass spectrum (ESI positive) of $[Ph(EO)_{16}MIM]_2[(S)\text{-BINAP-}(SO_3)_2]$ (**3b**)

3.10 Mass spectrum (ESI negative) of **3b**

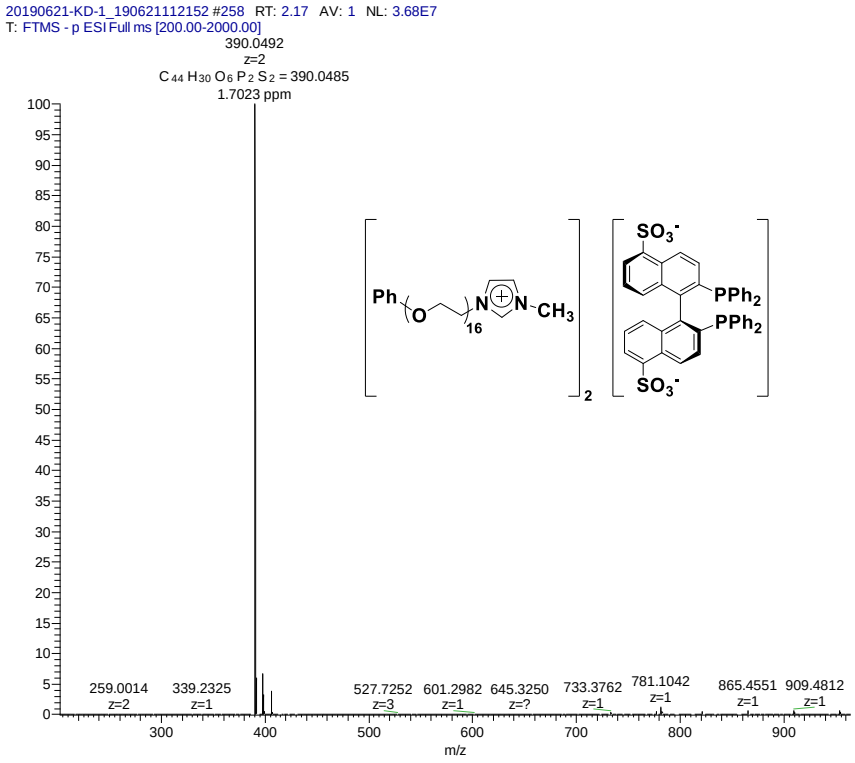

Figure S38. Mass spectrum (ESI negative) of $[Ph(EO)_{16}MIM]_2[(S)\text{-BINAP-}(SO_3)_2]$ (**3b**)

3.11 Mass spectrum (ESI positive) of **7**

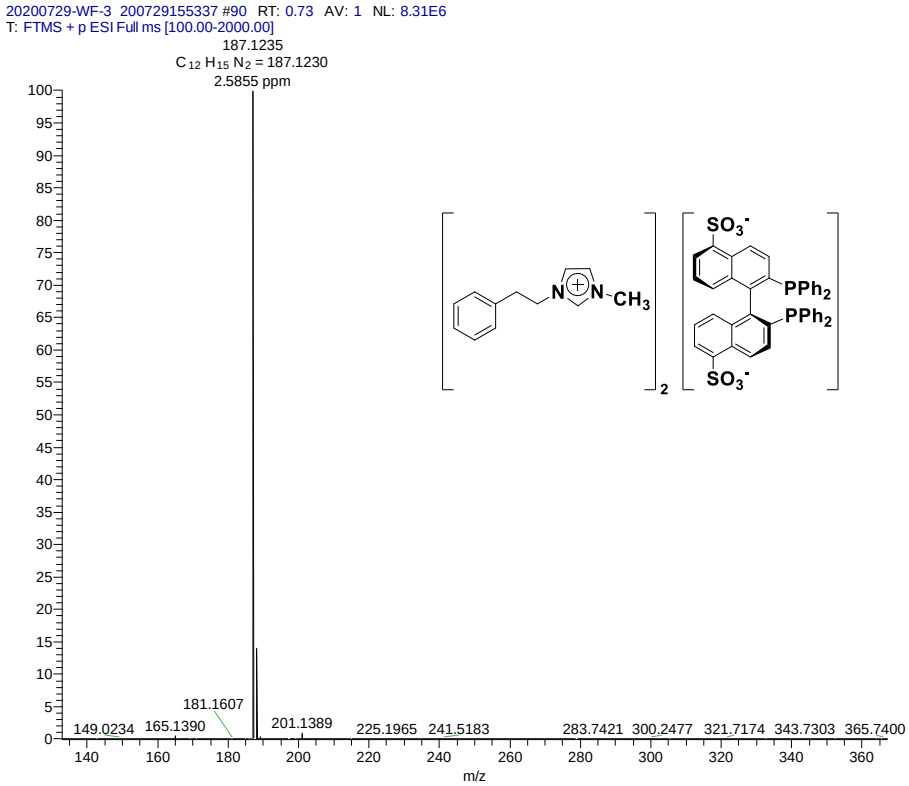

Figure S39. Mass spectrum (ESI positive) of $[Ph(CH_2)_2MIM]_2[(S)\text{-BINAP-}(SO_3)_2]$ (**7**)

3.12 Mass spectrum (ESI negative) of **7**

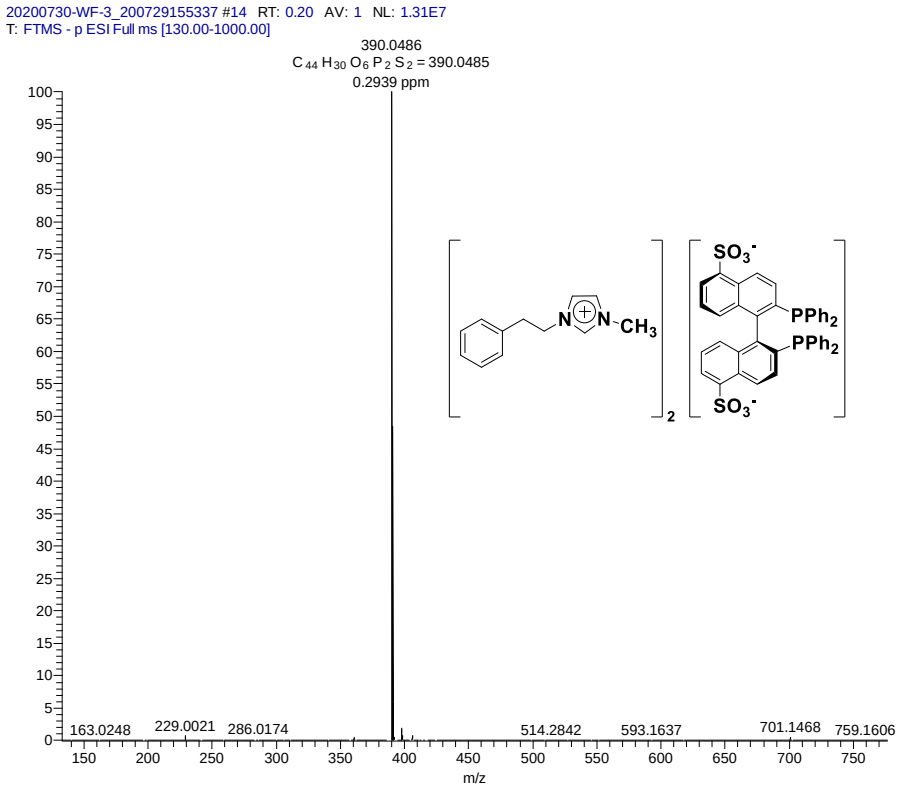

Figure S40. Mass spectrum (ESI negative) of $[Ph(CH_2)_2MIM]_2[(S)\text{-BINAP-}(SO_3)_2]$ (**7**)

3.13 Mass spectrum (ESI positive) of ethyl (*R*)-3-methoxy-3-(4'-methoxyphenyl) propanoate (**5j**) (Figure S40)

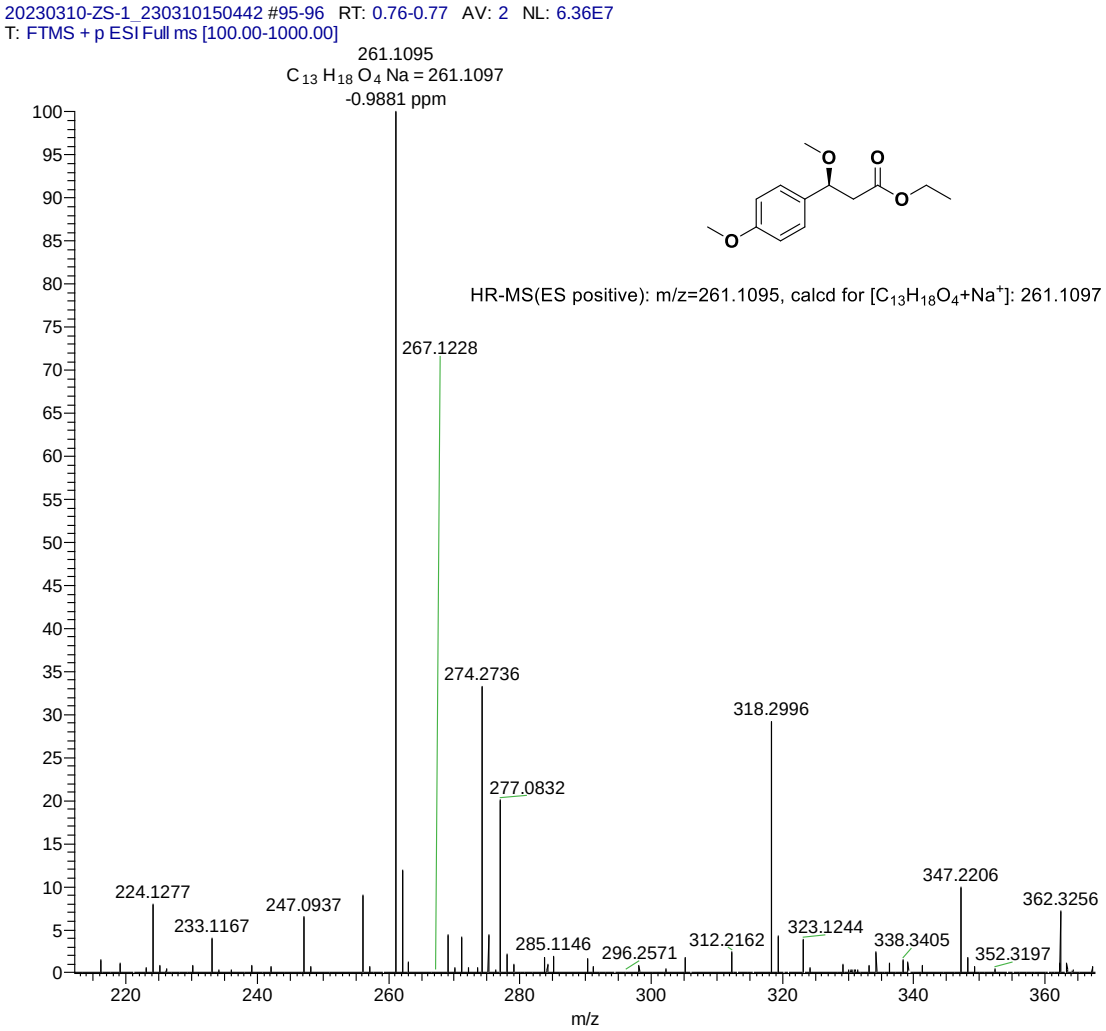

Figure S41. Mass spectrum (ESI positive) of ethyl (*R*)-3-methoxy-3-(4'-methoxyphenyl) propanoate (**5j**)

4 DSC and TG profiles of 3a and 3b

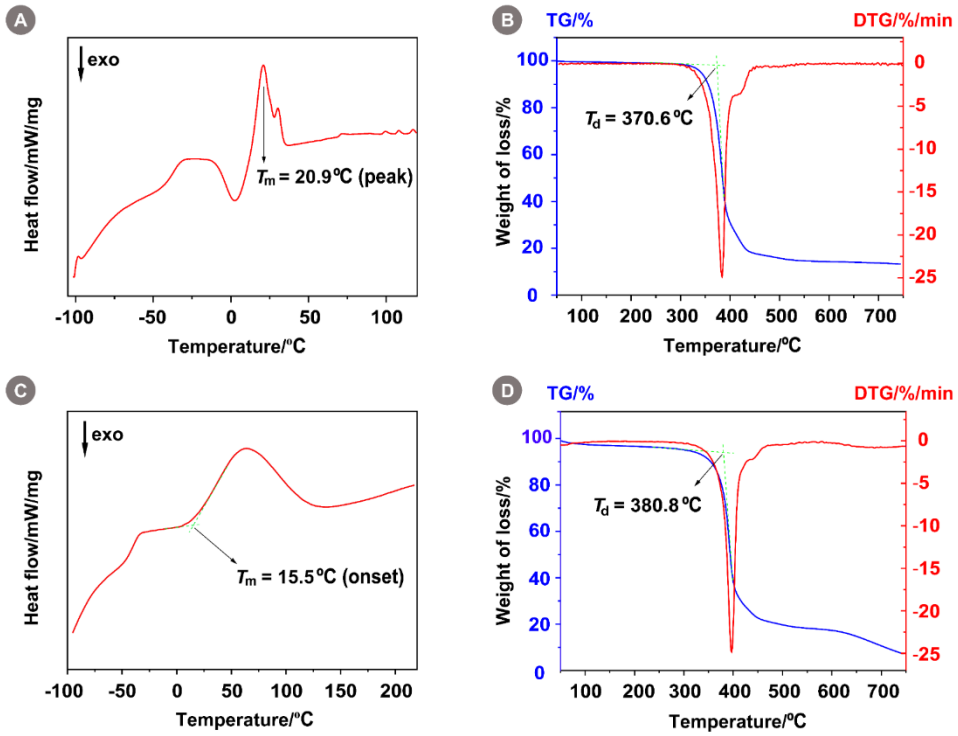

Figure S42. DSC and TG profiles of (A and B) **3a** and (C and D) **3b**

5 ^{31}P NMR spectra of Ru-1 and Ru-3b catalysts

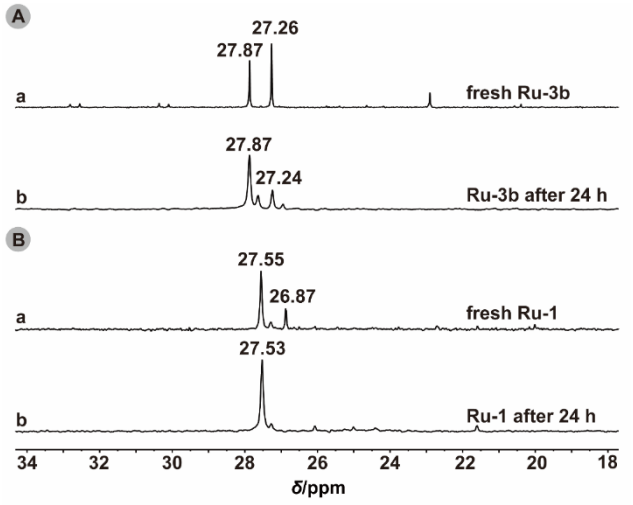

Figure S43. ^{31}P NMR spectra of (A) Ru-**3b** (161.9 MHz, DMSO-d_6, 22.7 mM, 298 K) and (B) Ru-**1** catalysts (202.4 MHz, DMSO-d_6, 22.7 mM, 298 K). (a) fresh catalysts; (b) catalysts in DMSO-d_6 for 24 h.

6 ^{31}P 2D-DOSY NMR spectrum of Ru-3b catalysts

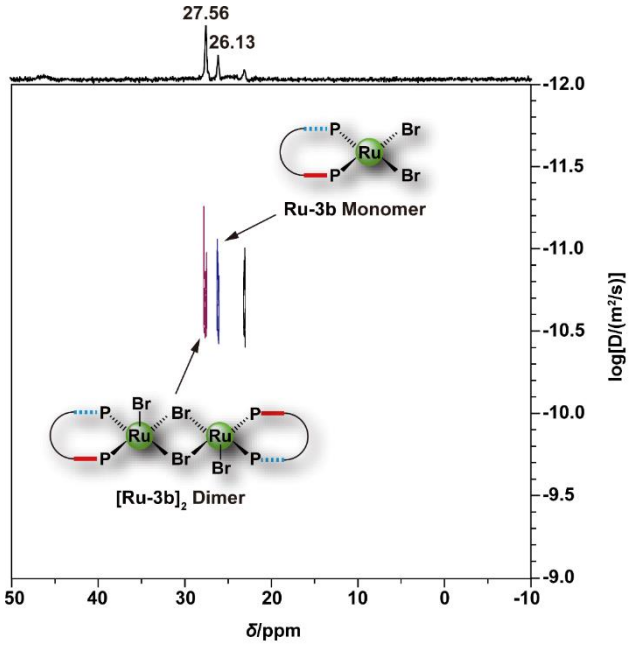

Figure S44. ^{31}P 2D-DOSY NMR spectrum of fresh Ru-**3b** catalyst (161.9 MHz, DMSO-d_6, 22.7 mM, 298 K, 2 h).

7 ^{31}P DOSY NMR spectra of Ru-1 and Ru-3b catalysts

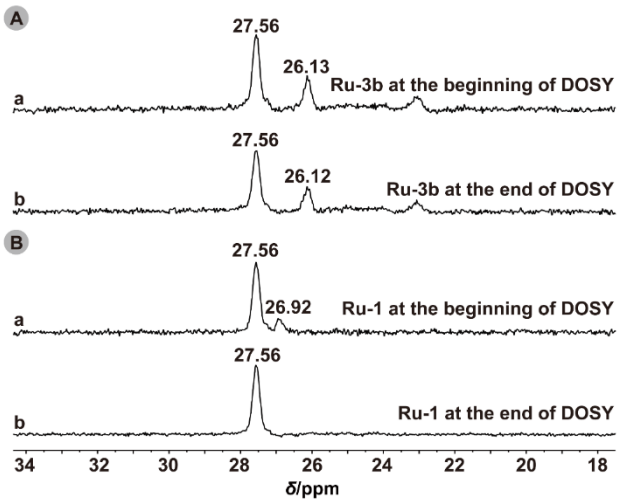

Figure S45. ^{31}P DOSY NMR spectra of (A) Ru-**3b** (161.9 MHz, DMSO-d_6, 22.7 mM, 298 K) and (B) Ru-**1** catalysts (161.9 MHz, DMSO-d_6, 22.7 mM, 298 K). (a) catalysts at the beginning of DOSY experiment; (b) catalysts at the end of DOSY experiment (2h).

8 Solvent Polarity Parameters as Linear Free-Energy Relationships

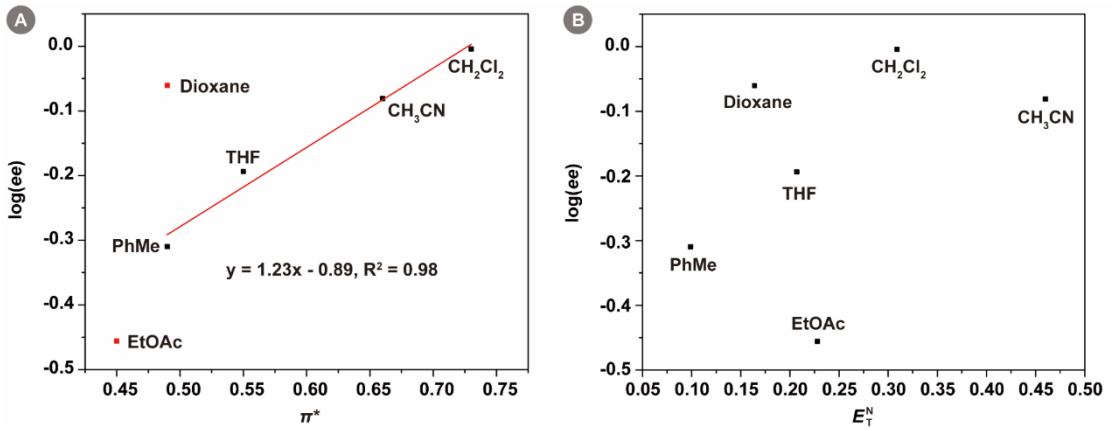

Figure S46. Correlation between aprotic solvent polarity parameters, (A) π^* and (B) E_T^N, and log(*ee*) in Ru-(*S*)-BINAP catalyzed asymmetric hydrogenation of MAA.

9 GC Spectra of Asymmetric Hydrogenation of *β*-Keto Esters

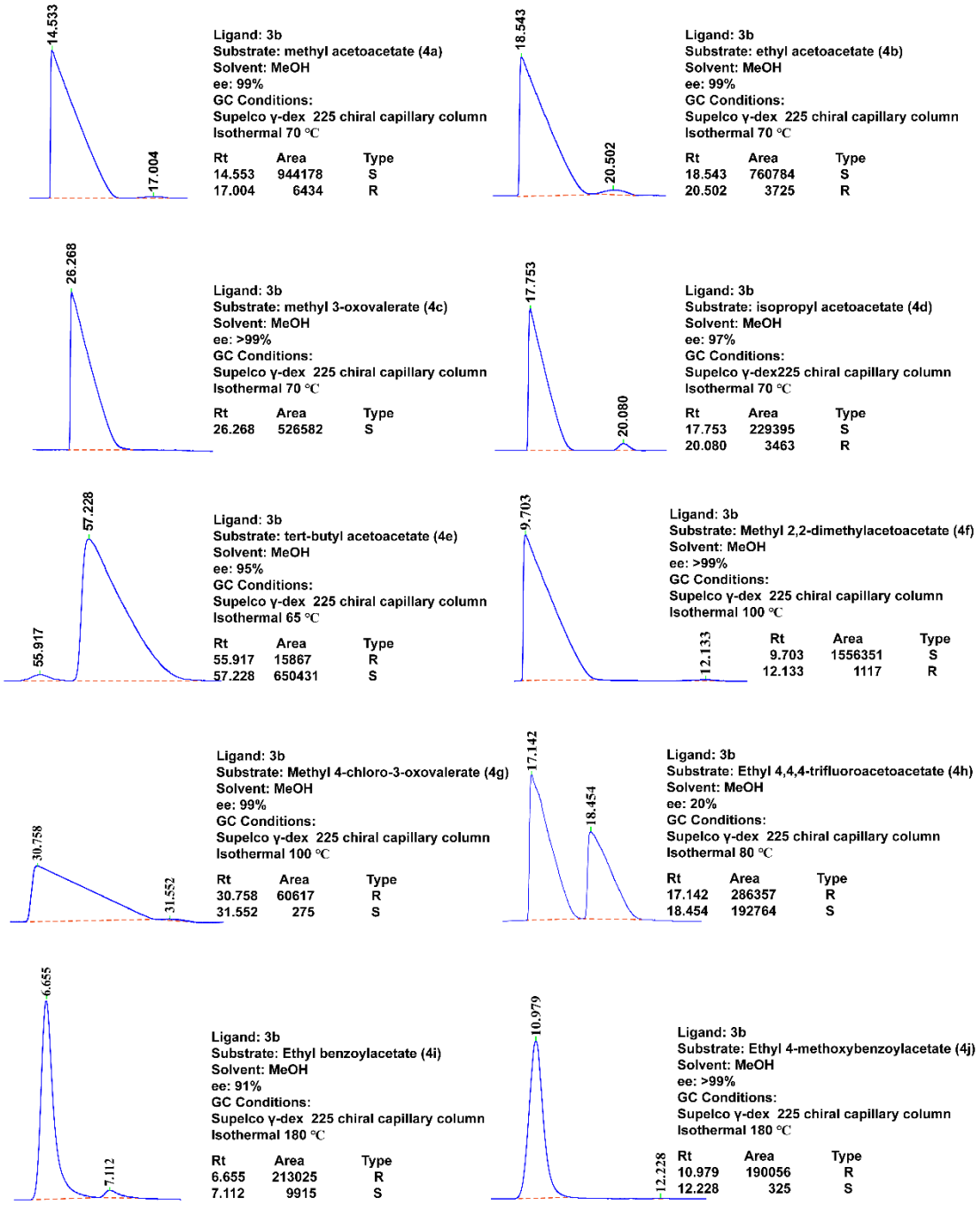

Figure S47. GC spectra of asymmetric hydrogenation of *β*-keto esters

10 Proposed catalytic cycle for enantioselective hydrogenation of ethyl benzoylacetate (4i) catalyzed by the Ru-**3b** or Ru-(*S*)-BINAP catalyst

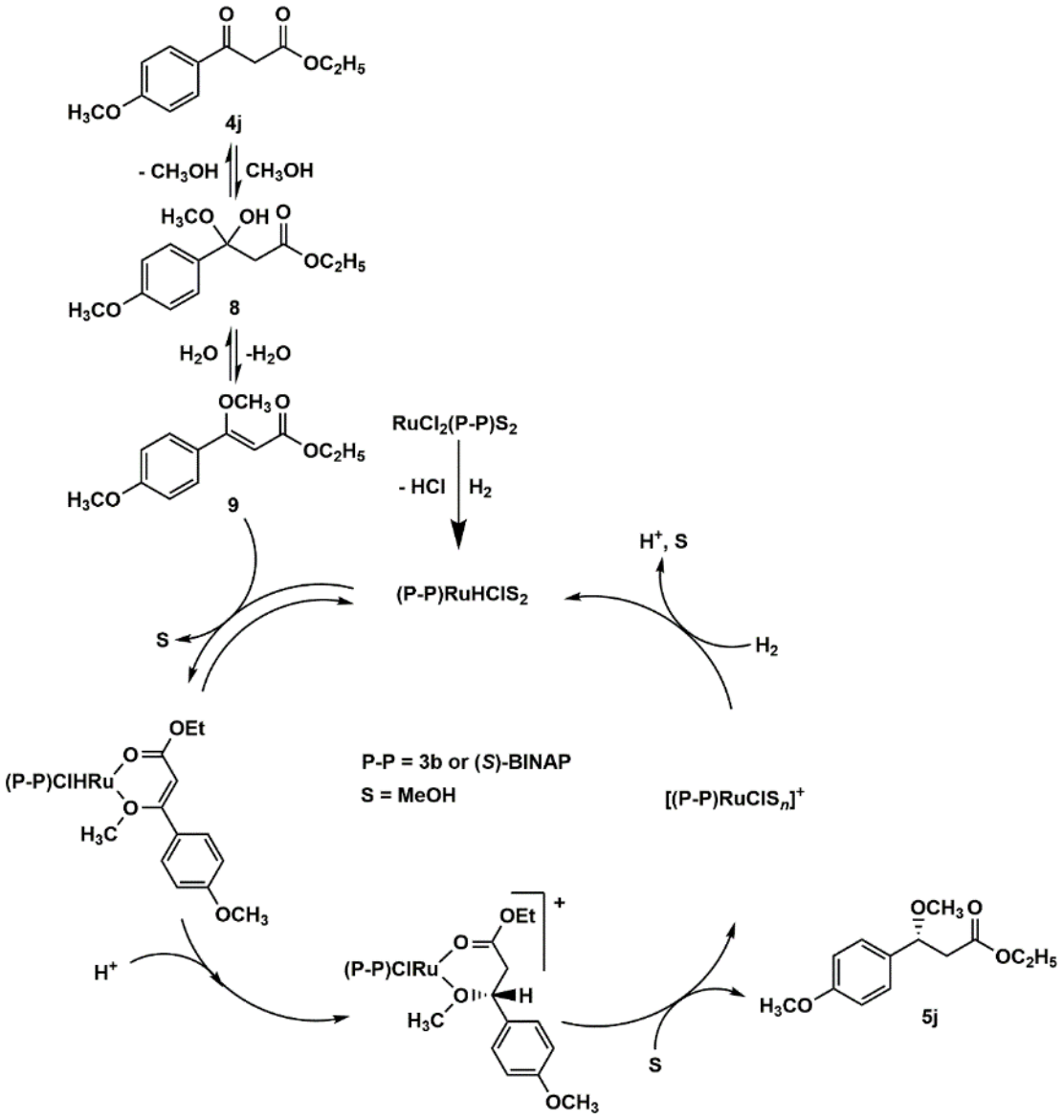

Figure S48. Proposed catalytic cycle for enantioselective hydrogenation of ethyl benzoylacetate (**4i**) catalyzed by Ru-**3b** or Ru-(*S*)-BINAP catalyst

11 Effect of excessive hydrobromic acid on activity of the neutral Ru-(*S*)-BINAP catalyst in enantioselective hydrogenation of MAA

Table S1. Effect of excessive hydrobromic acid on activity of the neutral Ru-(*S*)-BINAP catalyst in enantioselective hydrogenation of MAA

Entry	Ligand	Carrier IL	Yield (%)	*Ee* (%)	TOF_{30} (h^{-1})
1	(*S*)-BINAP	None	>99	93	2334

[a] Reaction conditions: [Ru(COD)(2-methylallyl)$_2$] 1.0 mg, 60 °C, H_2 4.6 MPa (at 60 °C), 1 h, catalyst loading 0.1 mol%, ligand/Ru = 1.2/1 (mol), Ru/HBr = 1/6.1 (mol), MeOH 2 mL.

12 Recycling experiment of Ru-BINAP/MeOH system for enantioselective hydrogenation of MAA

Table S2. A controlled experiment: recycling experiment of Ru-BINAP/MeOH system for enantioselective hydrogenation of MAA[a]

Entry	Reaction Medium	Ligand	Carrier IL/S (mol%)	Separation Mode[b]	Run	Yield (%)	*Ee* (%)	TOF[c] (h^{-1})	Ru Loss (%)
1	MeOH	BINAP	0	extraction	1	>99	99	500	15.3
2	MeOH	BINAP	0	extraction	2	50	85	250	—

[a] Reaction conditions: [Ru(COD)(2-methylallyl)$_2$] 1.0 mg, 60 °C, H_2 4.6 MPa (at 60°C), 2 h, catalyst loading 0.1 mol%, ligand/Ru = 1.2/1 (mol), Ru/HBr = 1/3.4 (mol), MeOH 2 mL. [b] A *n*-hexane extraction process was used to separate the product from the chiral catalyst. [c] Calculated based on the total reaction time.

13 Comparison of our HCBS system with state-of-the-art systems for enantioselective hydrogenation of *β*-keto esters

Table S3. Comparison of our HCBS system with state-of-the-art systems for enantioselective hydrogenation of *β*-keto esters

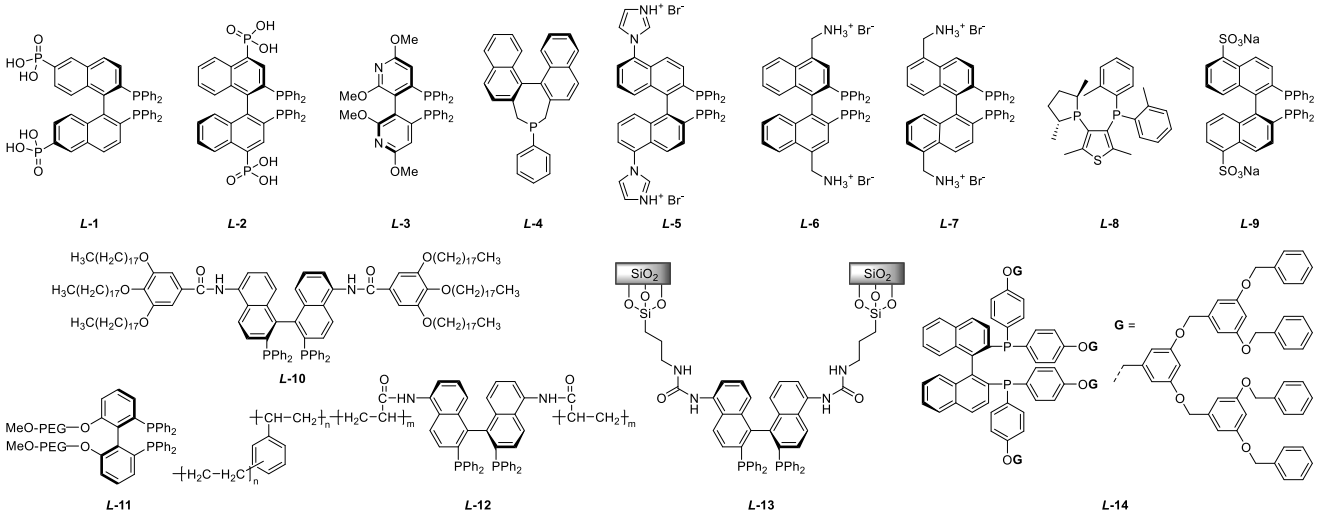

Entry	System	Reaction Medium	Ligand	Carrier IL/S[a] (mol%)	Separation Mode	TOF[b] (h^{-1})	*Ee* (%)	TTON	Ru Loss (%)	Ref.*
1[c]	IL-monophasic	[BMIM]BF_4/MeOH	*L*-**1**	580	extraction	4.5	98.3	440	0.02	7a
2[c]	IL-monophasic	[BMIM]PF_6/MeOH	*L*-**2**	371	extraction	4.5	99.0	521	0.01	7a
3[d]	IL-monophasic	[BMIM]BF_4/MeOH	*L*-**3**	116	extraction	5.0	>99	577	—	6a
4[e]	IL-monophasic	[NMe_2(EtOH)$_2$]/MeOH	*L*-**4**	511	distillation	5.5	93.0	365	—	7e
5[f]	IL-monophasic	[BMIM]NTf_2/MeOH	*L*-**5**	769	extraction	5.0-50	98	400	0.2-4.6	18a
6[f]	IL-monophasic	[BMIM]NTf_2/MeOH	BINAP	769	extraction	5.0-50	98	228	4.63	18a
7[g]	IL-monophasic	$N_{6222}NTf_2$/MeOH	BINAP	—	extraction	1235[h]	98.3	—	—	7d
8[i]	IL-monophasic	[BMIM]BF_4/$scCO_2$	BINAP	209	extraction	100	97	—	—	39
9[j]	IL-biphasic	[BMIM]BF_4	*L*-**6**	31	extraction	66.7	86	2000	—	7b
10[j]	IL-biphasic	[BPy]NTf_2	*L*-**7**	20	extraction	66.7	83	—	—	7b
11[k]	IL-biphasic	[BMIM]PF_6/*i*-PrOH	BINAP	3469	extraction	21	97	14	0	4g
12[l]	SILP-catalysis	SiO_2-[EMIM]NTf_2/MeOH	*L*-**8**	—	solid/liquid	—	75-80	2500	—	40
13[m]	aqueous biphasic	H_2O	*L*-**6**	*none*	extraction	66.7	99	8000	—	26e
14[n]	aqueous biphasic	H_2O	*L*-**9**	*none*	extraction	50/981[o]	94	5000	—	27
15[p]	thermoregulated	EtOH/1,4-dioxane	*L*-**10**	*none*	cooling	10	97.8	383	1.78	41
16[q]	MeO-PEG-supported	EtOH	*L*-**11**	*none*	precipitation	25	98	97	—	30k
17[r]	mesoporous polymer	MeOH	*L*-**12**	*none*	solid/liquid	100	94.6	14000	—	42
18[s]	dendrimer-supported	CH_2Cl_2/MeOH	*L*-**14**	*none*	precipitation	7.9	92	1462	—	43
19[t]	SiO_2-supported	MeOH	*L*-**13**	*none*	solid/liquid	21	>99	5000	0.18	44
20[u]	C-FDU-12-encapsulated	MeOH	BINAP	*none*	solid/liquid	42/299[v] 500	97	4000	—	45
21[w]	HCBS system	MeOH	**3b**	0	extraction	3913[x] 1442[y]	99	17000[z]	0.08-0.09	this work

[a] Molar ratio of carrier IL to substrate. [b] Calculated based on the total reaction time. [c] r.t., 10.2 MPa, 22 h, S/Ru = 100/1, *L*/Ru = 1.1/1, [$RuCl_2(C_6H_6)]_2$, MAA. [d] r.t., 6.8 MPa, 20 h, S/Ru = 100/1, MAA. [e] 80 °C, 1 MPa, 18 h, S/Ru = 100/1, *L*/Ru = 2/1, [Ru(COD)(2-methylallyl)$_2$], MAA. [f] 60 °C, 4 MPa, 20 h, S/Ru = 1000/1, *L*/Ru = 1/1, [Ru(COD)(2-methylallyl)$_2$], MAA. [g] 60 °C, 5 MPa, S/Ru = 1580/1, 1 wt.% N_{6222}Br, [$RuCl_2$(*p*-cymen)]$_2$, MAA. [h] TOF value at 90% conversion. [i] 75 °C, 2.7 MPa (H_2), 8 MPa (CO_2), 2 h, S/Ru = 200/1, *L*/Ru = 1.5/1, [$RuCl_2(C_6H_6)]_2$, ethyl 4-chloro-3-oxobutyrate. [j] 50 °C, 4 MPa, 15 h, S/Ru = 1000/1, ethyl acetoacetate (EAA). [k] 60 °C, 4 MPa, 20 min, S/Ru = 140/1, MAA. [l] A continuous gas-phase reaction: 105 °C, 1 MPa, 70 h, [Ru(COD)(2-methylallyl)$_2$], MAA. [m] 50 °C, 4 MPa, 15 h, S/Ru = 1000/1, EAA. [n] 60 °C, 4 MPa, S/Ru = 1000/1, NaI/Ru = 100/1, [RuI_2(*p*-cymen)]$_2$, MAA. [o] TOF value at 30% conversion. [p] 60 °C, 4 MPa, 10 h, S/Ru = 100/1, *L*/Ru = 1.1/1, [$RuCl_2(C_6H_6)]_2$, MAA. [q] 55-60 °C, 0.1 MPa, 2 h, S/Ru = 50/1, *L*/Ru = 1/1, [Ru(COD)(2-methylallyl)$_2$], EAA. [r] 50 °C, 2 MPa, 20 h, S/Ru = 2000/1, *L*/Ru = 1/1, [$RuCl_2(C_6H_6)]_2$, MAA. [s] 60 °C, 5 MPa, 24 h, S/Ru = 200/1, 5 mol% TsOH, methyl benzoylacetate. [t] 50 °C, 4 MPa, 48 h, S/Ru = 1000/1, [$RuCl_2(C_6H_6)]_2$, MAA. [u] 50 °C, 4 MPa, 24 h, S/Ru = 1000/1, MAA. [v] TOF value at the initial 1 h. [w] 60 °C, 4.6 MPa (at 60°C), 2 h, S/Ru = 1000/1, *L*/Ru = 1.2/1, [Ru(COD)(2-methylallyl)$_2$], MAA. [x] TOF value at 30% conversion. [y] TOF value at complete conversion. [z] After two times of **3b** supplementation, the total molar ratio of **3b** to Ru is 2/1. * The references are consistent with the main text.